School of Science

Department of Geology & Geoenvironment

Spectroscopic study of REE cyclosilicate (eudialyte-type) minerals

Stavros Kousaris (BSc Thesis)

Supervisor: Prof. A. Godelitsas

Athens, 2022

Outline

This BSc Thesis concerns the study of REE cyclosilicate (eudialyte-type) minerals, originating in Greenland and Russia, by spectroscopic techniques (Mössbauer spectroscopy, ICP-OES/MS, and γ-ray spectrometry). The aim was to investigate structural and compositional features of certain elements (e.g. Fe) with emphasis in REE and actinides (U, Th). At the same time the minerals were complementary characterized by PXRD and SEM-EDS. The results constitute a contribution to the mineralogy and geochemistry of a geological material exhibiting an importance for the modern industry/technology, as source of critical metals (REE), and also arising environmental issues due to radioactivity content.

Keywords: Eudialyte; rare earth elements (REE); critical metals; Greenland; Russia; actinides; uranium; thorium; Spectroscopy; Gamma-rays.

1. Introduction

The eudialyte-group minerals are Na-Ca-Zr-cyclosilicates that accommodate various elements in their complicated crystal structure. In addition to the major elements Na, Ca, Zr and Si, they host considerable amounts of Fe, Mn, REE, Y, Nb, Hf, Ti, K, Sr and Ti as well as Cl, F, H_2O and OH groups (**Fig. 1**; see Johnsen et al. 2003 and references therein; Borst et al. 2020 and references therein).

The IMA-accepted formula for the eudialyte group is: $N_{15-16}[M1]_6[M2]_3[M3][M4]Z_3Si_{24}O_{66-73}(\Theta)_{0-9}(X)_2$, where: $N = Na^+$, K^+, Sr^{2+}, Ca^{2+}, REE^{3+}, $\square$ (vacancy), Ba^{2+}, Mn^{2+} or H_3O^+; $M1 = Ca^{2+}$, REE^{3+}, Mn^{2+}, Fe^{2+}, Na^+, Sr^{2+}; $M2 = Fe^{2+}$, Mn^{2+}, Na^+, $\square$, H_3O^+, Zr^{4+}, Ta^{5+}, Ti^{4+}, K^+, Ba^{2+} or Fe^{3+}; $M3/4 = Si^{4+}$, Al^{3+}, Nb^{5+}, Ti^{4+}, W^{6+} or Na^+, $Z = Zr^{4+}$, Hf^{4+}, Ti^{4+} or Nb^{5+}; $\Theta = H_2O$, OH^-, O^{2-}, CO_3^{2-}, SO_4^{2-} or SiO_4^{4-}; and $X = Cl^-$, F^- or OH^- (Johnsen *et al.*, 2003).
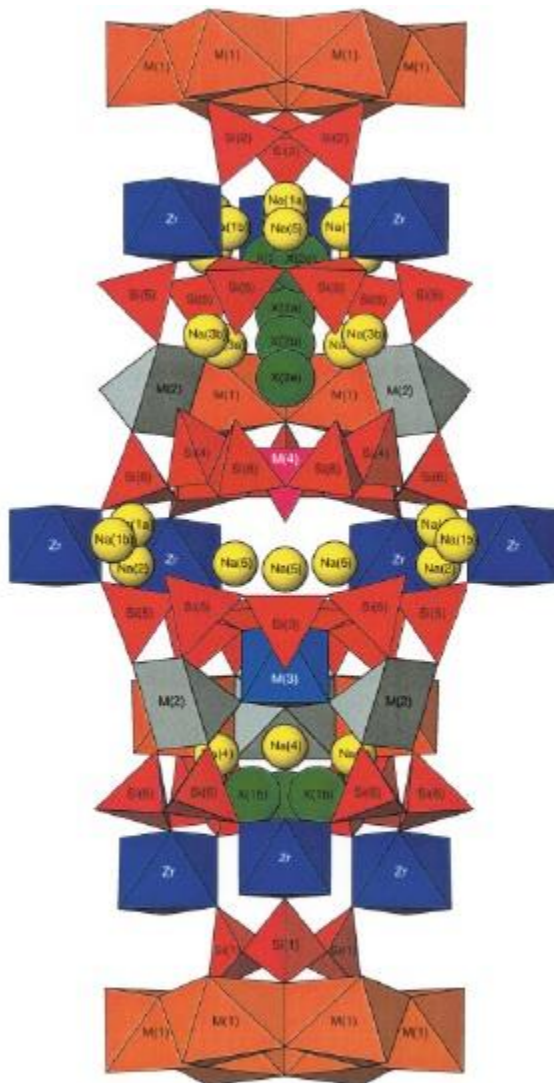
Fig. 3. Polyhedral model of the *R3m* eudialyte structure showing the sequence of layers along a triad axis from one ring of [M(1)O₆] octahedra to another. The structure is viewed approximately along [210].
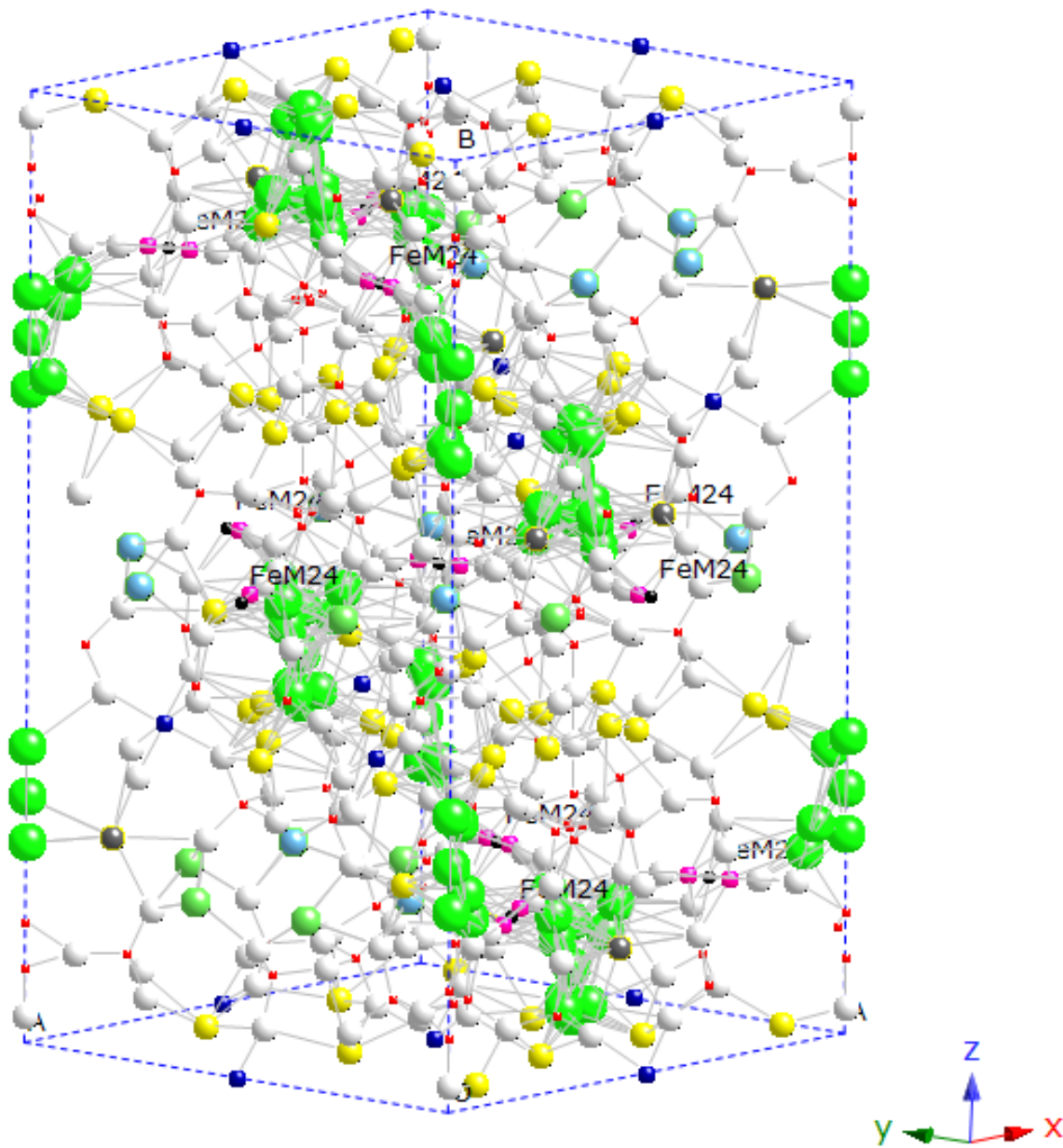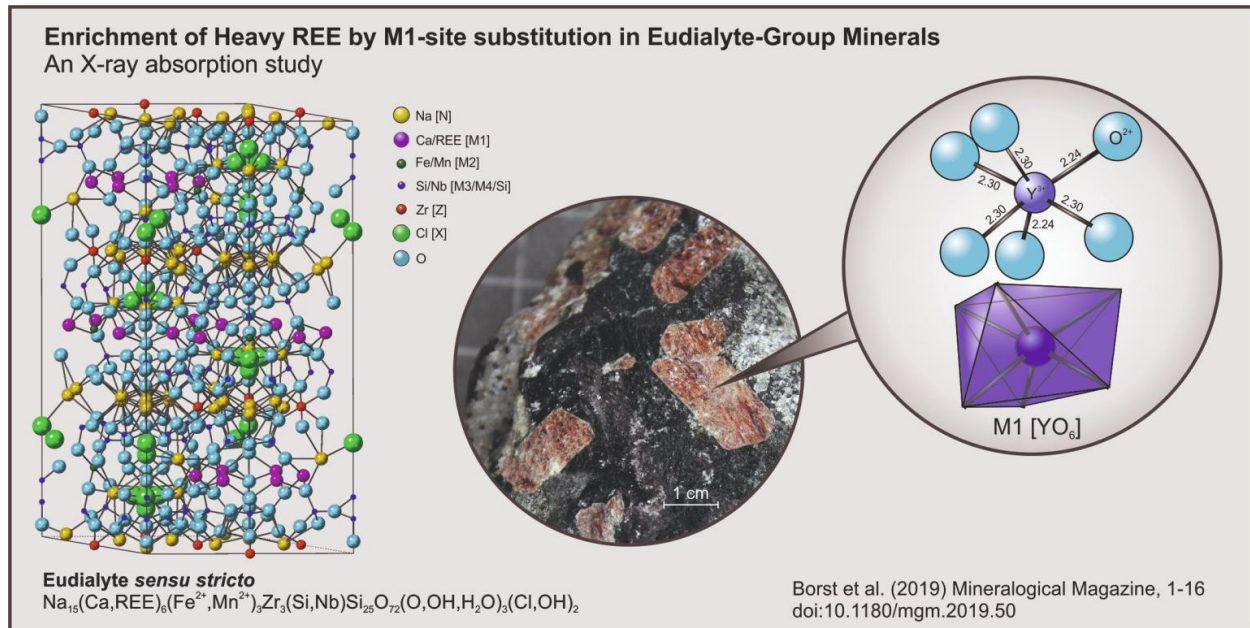
Fig. 1: The chemical composition and structure of Eudialyte (Johnsen et al. 2003 and references therein; Borst et al. 2020 and references therein)

Eudialyte-group minerals have been considered as important sources of critical metals, and particularly Rare Earth Elements (REE). Major deposits occur in specific types of igneous rocks in some areas of the world including Greenland (constituent country of the Kingdom of Denmark) and Russia -Kola Peninsula- (**Figs. 2-6**).
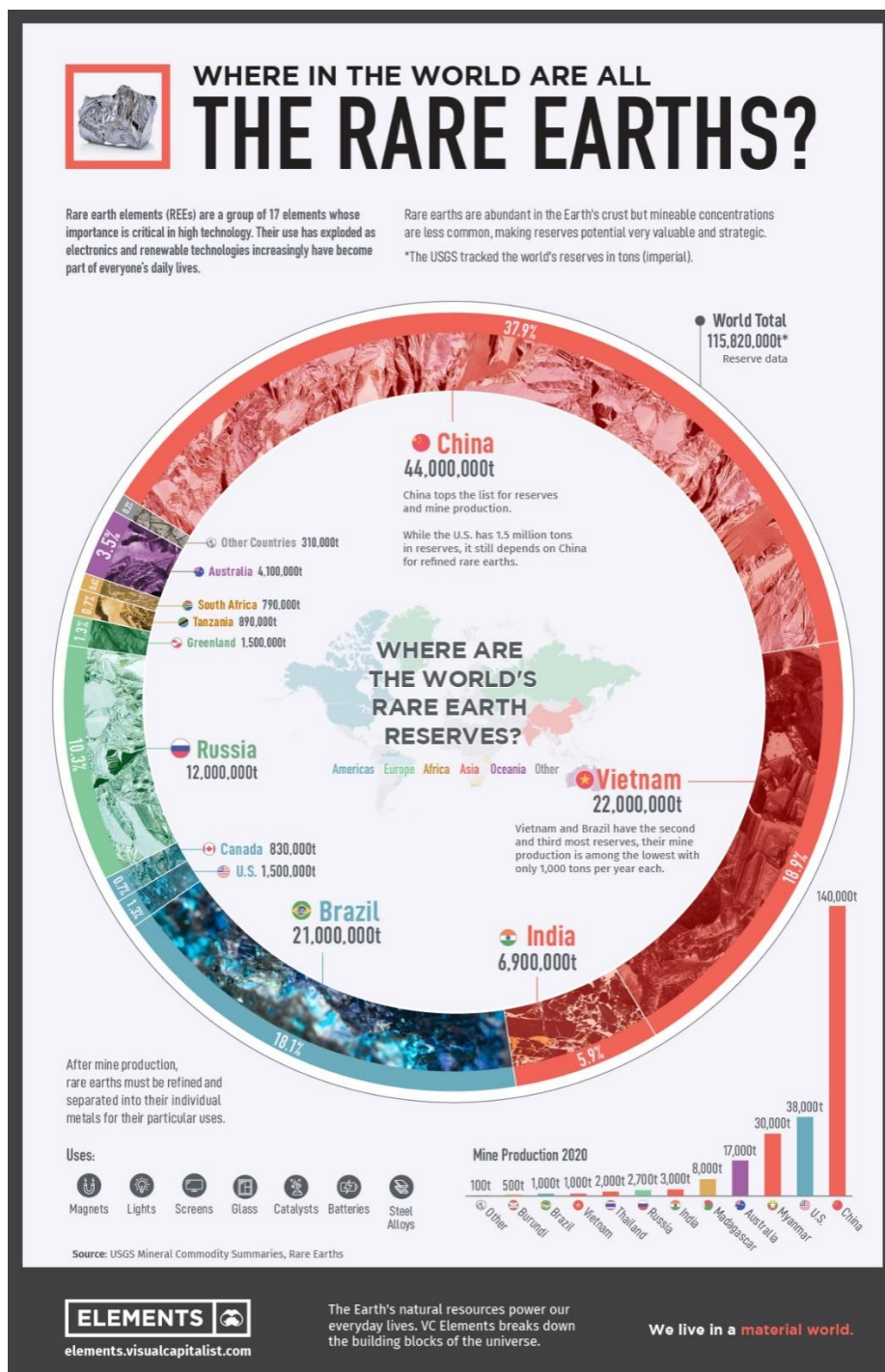
Fig. 2: Major REE suppliers/reverses in the world and the particular uses of metals
(https://www.visualcapitalist.com/rare-earth-elements-where-in-the-world-are-they/)
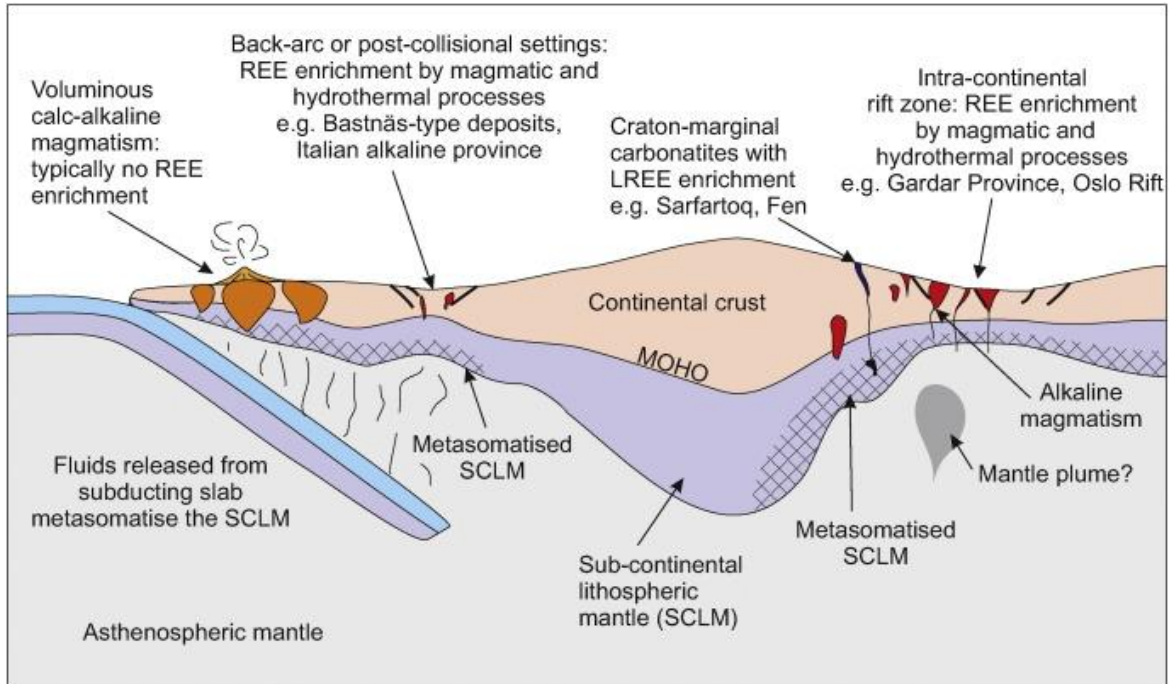
Fig. 3: Schematic diagram to illustrate the main environments of formation of alkaline igneous rocks and carbonatites, major hosts of many REE deposits (Goodenough et al. 2016 and references therein)
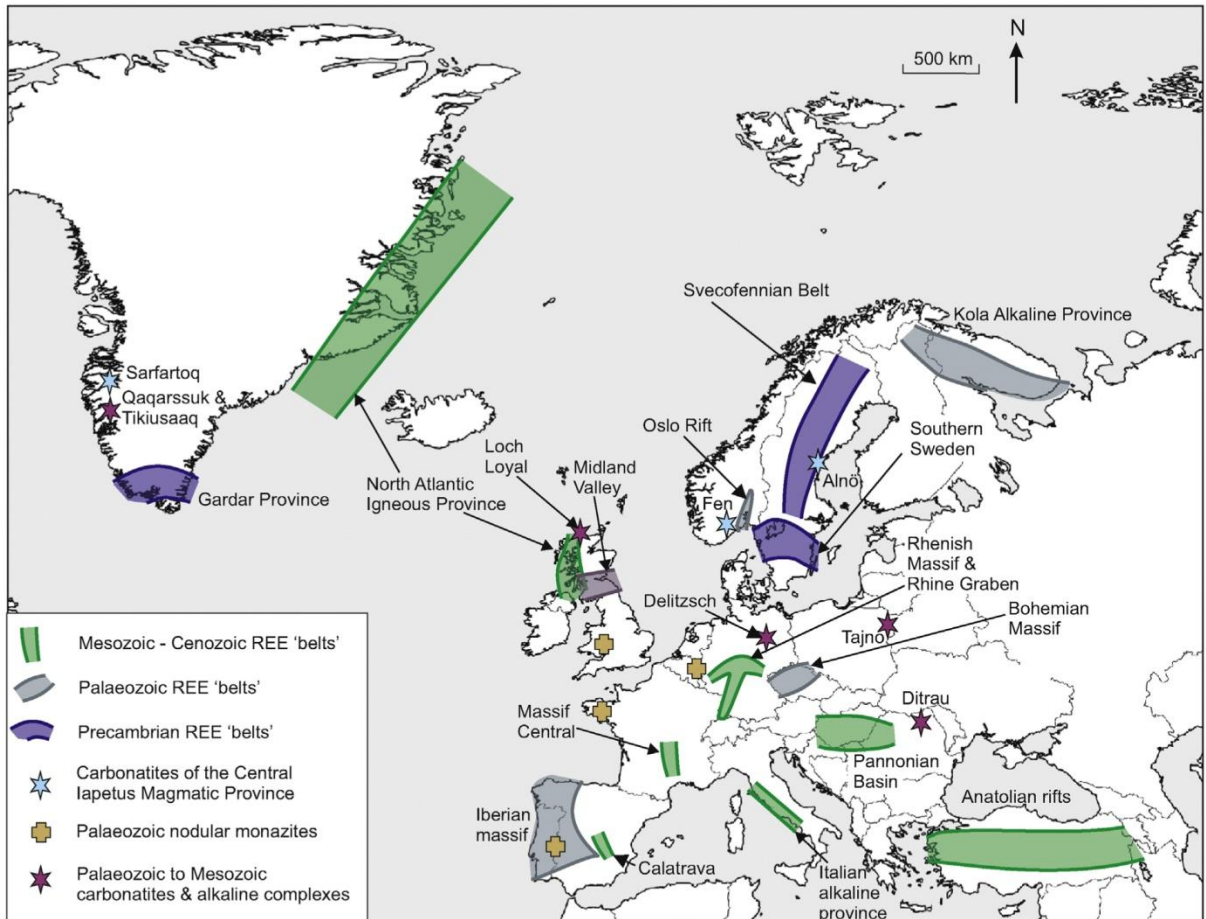
Fig 4: Overview map of Europe showing the approximate extent of the key REE metallogenetic belts. Notable REE deposits and occurrences that do not fall within a distinct belt and are not shown on other maps are indicated by symbols. (Goodenough et al. 2016 and references therein)
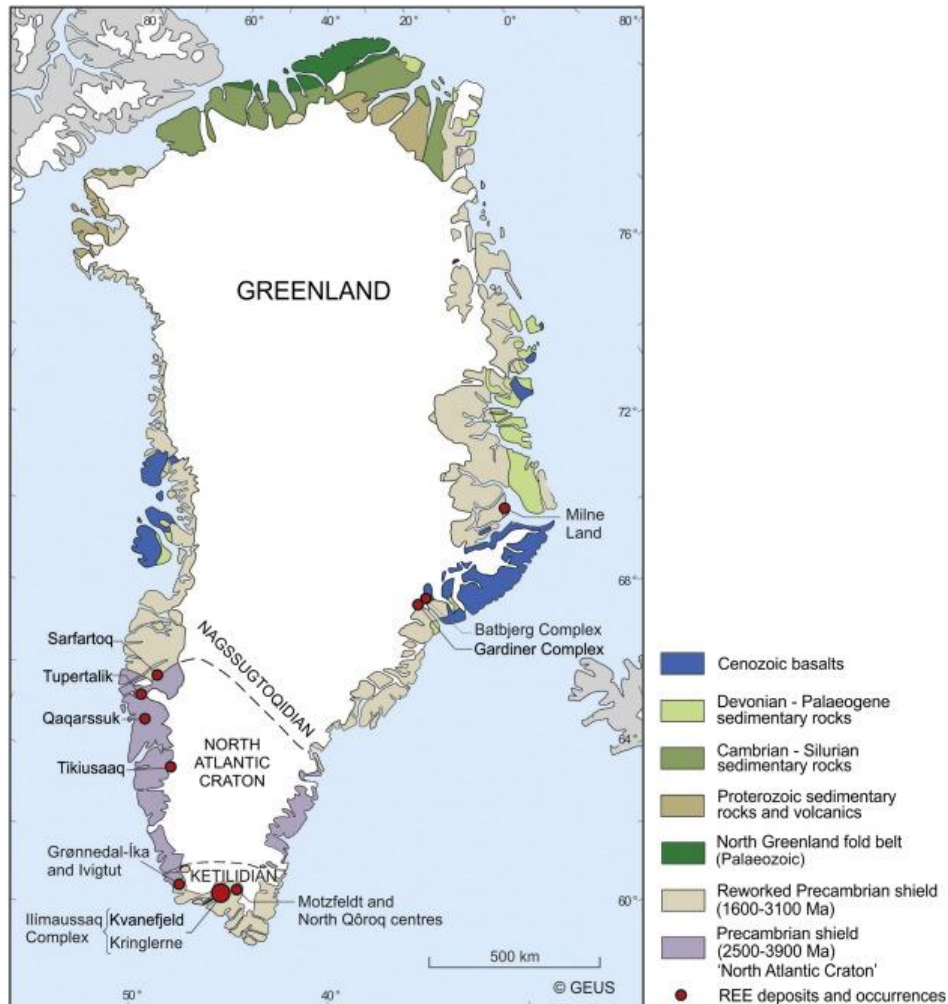
Fig 5: Simplified geological map of Greenland showing the main REE deposits and occurrences. Base geological map from GEUS. (Goodenough et al. 2016 and references therein)
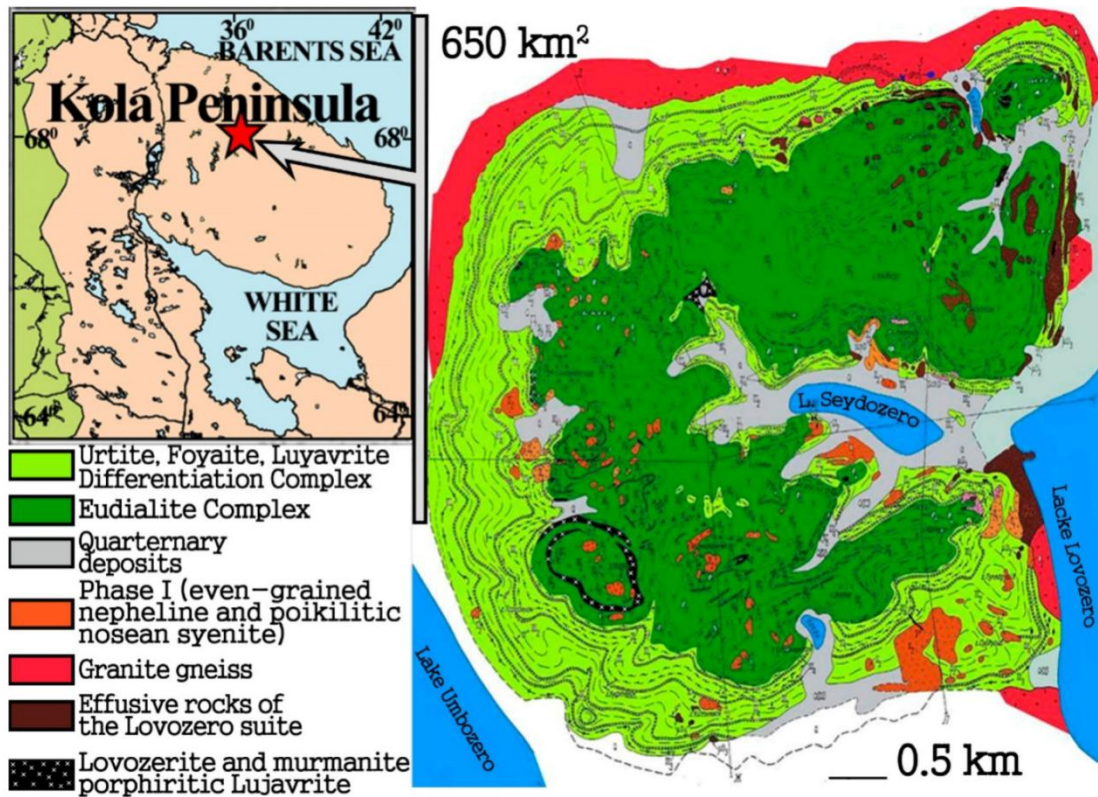
Fig 6: Geological map of the Lovozero intrusion with inset showing location of Lovozero (star) within the Kola Peninsula (Kogarko and Nielsen 2020 and references therein)

According to the literature, despite the fact that eudialyte is a very promising mineral for REE extraction, there are environmental issues related to radioactivity due to considerable actinide (and also ^{40}K) content. Such case was the temporary ban of uranium mining in Greenland, recently (https://www.reuters.com/world/americas/greenland-bans-uranium-mining-halting-rare-earths-project-2021-11-10/). Thus, the final purpose of the present Thesis, except of contributing to the mineralogy and geochemistry of the mineral, was to re-evaluate the radionuclides occurring in typical eudialyte samples.

2. Materials and Methods

2.1. Samples

The samples (**Fig. 7**), obtained from the personal mineral collection of Dr. A. Godelitsas, included eudialyte crystals into igneous rocks from Greenland and Russia (Kola peninsula). Pure eudialyte crystals (Eudialyte Russia: **R**; Eudialyte Greenland: **G**) were separated after careful crushing using a stereomicroscope. The final material was checked by PXRD.

Fig. 7: Typical eudialyte samples(R) examined in the present study

2.2. PXRD

The powder X-ray Diffraction (PXRD) study was performed using a Siemens D5005 –now Bruker AXS- diffractometer, CuK_α radiation at 40 kV and 40 mA. The evaluation of the diffragtograms was carried out using the EVA 10.0 program of the Bruker DIFFRACplus software package and the MATCH! (Crystal Impact) software.

2.3. Microscopic study (SEM-EDS)

The Scanning Electron Microscopic study and the corresponding Energy Dispersive microanalyses (SEM-EDS) were performed using a Jeol JSM-5600 equipped with an Oxford EDS (**Fig. 8**), as well as a Jeol JSM-6300F equipped with an Oxford EDS.
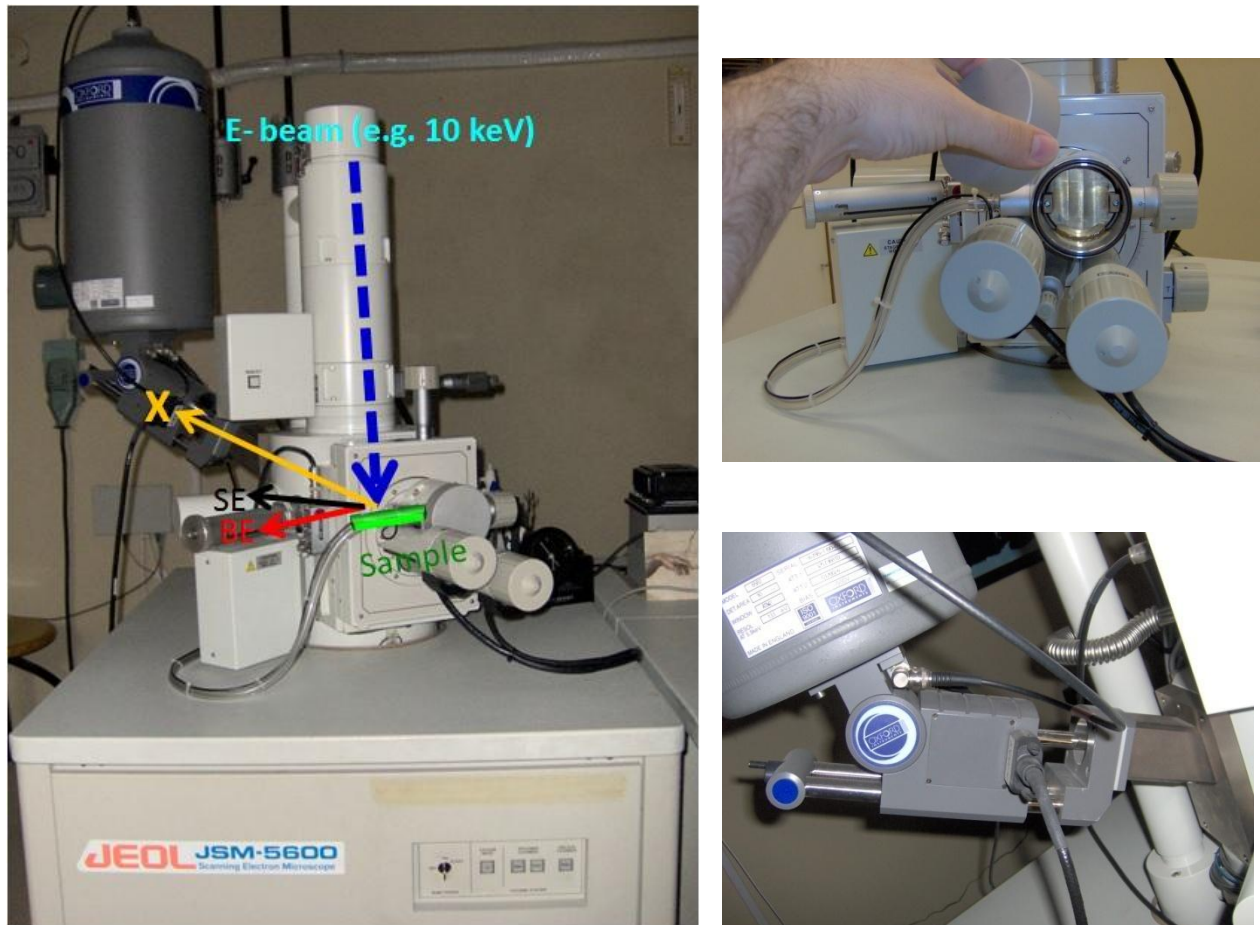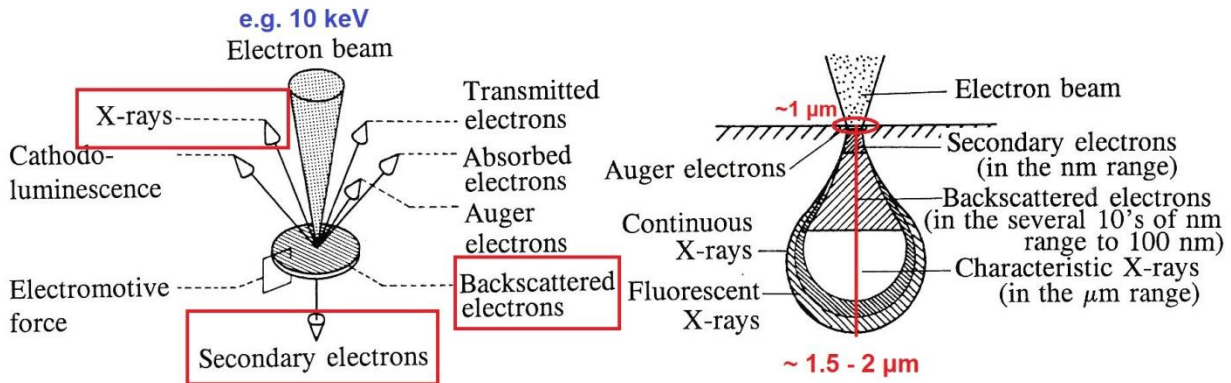
Fig. 8: A typical SEM-EDS system

The working principle of the method is based on the interaction of the samples atoms with a focused beam of electrons, which produces a number of secondary electrons depending on the specimens topography. The detection of the secondary electrons that are emitted by the sample's atoms results in the formation of an image displaying the topography of the surface. The X-ray spectrum emitted by a solid sample bombarded with a focused beam of electrons is used to obtain a localized chemical analysis. Characteristic X-rays result from the electron transitions between inner orbits that produce X-ray photons with energy equivalent to the difference between the levels. Energy-dispersive spectrometers (EDSs) employ pulse height analysis, a detector giving output pulses proportional in height to the X-ray photon energy is used in conjunction with a pulse height analyzer.Incident X-ray photons cause ionization in the detector, producing an electrical charge, which is amplified by a sensitive preamplifier located close to the detector (e.g. Russ, 1984). The electron probe analysis can only reach shallow depths, the polishing of the specimen is required so the surface roughness doesn't affect the results. The required information to identify the specific energy of the characteristic X-ray peaks for each

element in performing qualitative X-ray analysis is available in the form of a computer database.The fact that the total spectrum of interest, from 0.1 keV to the beam energy (e.g., 20 keV) can be acquired in a short time (10 - 100 s) allows for a rapid evaluation of the specimen. Images of the samples on different scales were taken along with the ED spectrum displaying the distribution of chemical elements with a mark on the sight of chemical analysis. The ED spectrum is displayed in digitized form with the x-axis representing X-ray energy in channels 20 eV wide and the y-axis representing the number of counts per channel. An X-ray line is broadened by the response of the system, producing a Gaussian profile. Energy resolution is defined as the full width of the peak at half maximum height.

2.4. Analyses (ICP-OES/MS and Leco)

Bulk analyses for major and trace elements were performed using a Perkin Elmer ICP-OES and a Perkin Elmer Sciex Elan 9000 ICP-MS following a $LiBO_2/LiB_4O_7$ fusion and HNO_3digestion of two 0.2 g samples. The chemical composition of investigated eudialyte composited samples, were achieved using strict QA/QC procedures including, of course, three analytical replicates. Blanks (analytical and method), duplicates and standard geological and synthetic reference materials provided a measure of background noise, accuracy and precision. Total carbon (C) and sulfur (S) concentration were measured by Leco.

2.5. Spectroscopic measurements (Mössbauer and γ-ray spectrometry)

[57]Fe Mössbauer spectra of the samples were recorded in transmission geometry at 300 K and at 10 K using a constant-acceleration Mössbauer spectrometer (**Fig. 9**) equipped with a [57]Co (Rh) source kept at room temperature (RT).
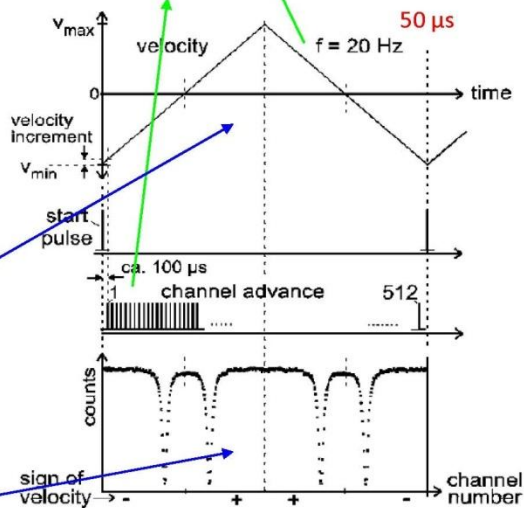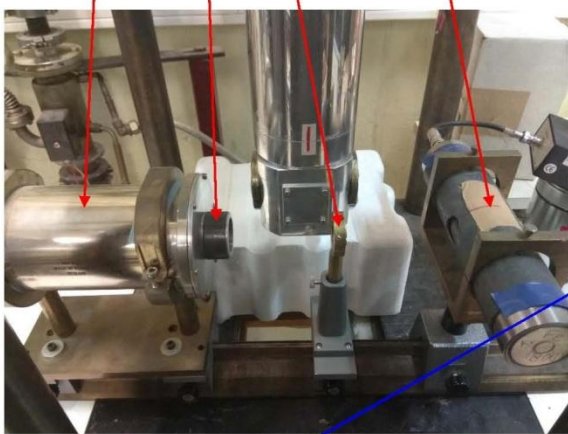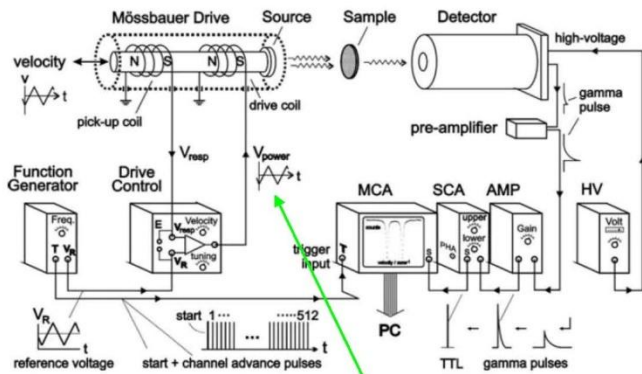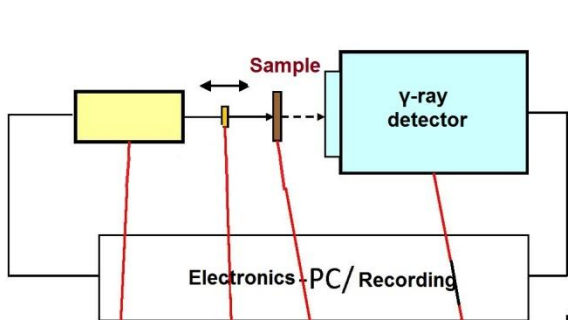
T=50 ms (1 $_{day}$ =1.728x10^6 T).
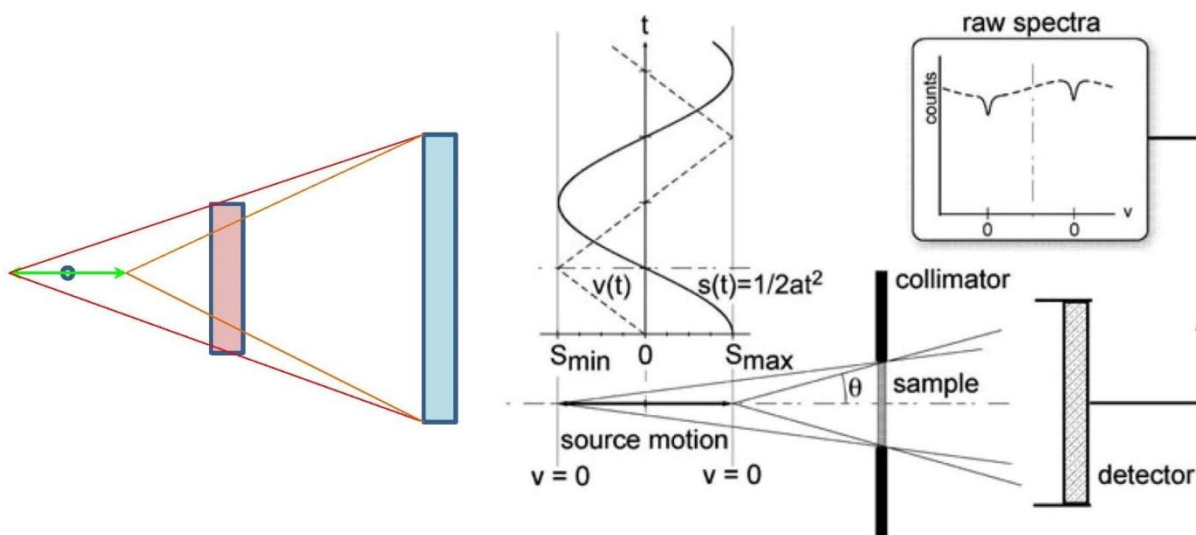
Fig. 9: The Mössbauer spectrometry set-up.

Gamma-ray spectrometry (**Fig. 10**) was applied for the determination of natural and radionuclides activity concentrations of the eudialyte minerals. The measurements were performed by means of a HPGe n-type detector (BE2020 Canberra) with 9% nominal relative efficiency and 1,9 keV energy resolution at 1.33 MeV, along with a computerized MCA system (DSA-1000 Model and Gennie-2000® software by Canberra) for the data acquisition. A cylindrical lead shield surrounded the detector in order to reduce the ambient gamma-ray background. The energy-dependent detection efficiency was determined using a [152]Eu reference source. Two samples where properly prepared and measured for 47 hours (R) and 92 hours (G) , whereas a phantom sample was also used in order to extract the background contribution from the experimental spectra.

Fig. 10: The γ-ray spectrometry system

3. Results and Discussion

3.1 PXRD

The PXRD patterns for the selected eudialyte minerals (G and R) are presented in **Fig. 11** and **Fig. 12**. According to the patterns, the materials consist of typical eudialyte, without significant (within the error of the technique) crystalline solid impurities. That is in accordance with Mössbauer spectra (see Section 3.3 below). However, various secondary minor phases in the G sample (detected by SEM-EDS; see below) and zircon and pyrite inclusions in the R sample (also detected by SEM-EDS) have not been recorded in the PXRD patterns.
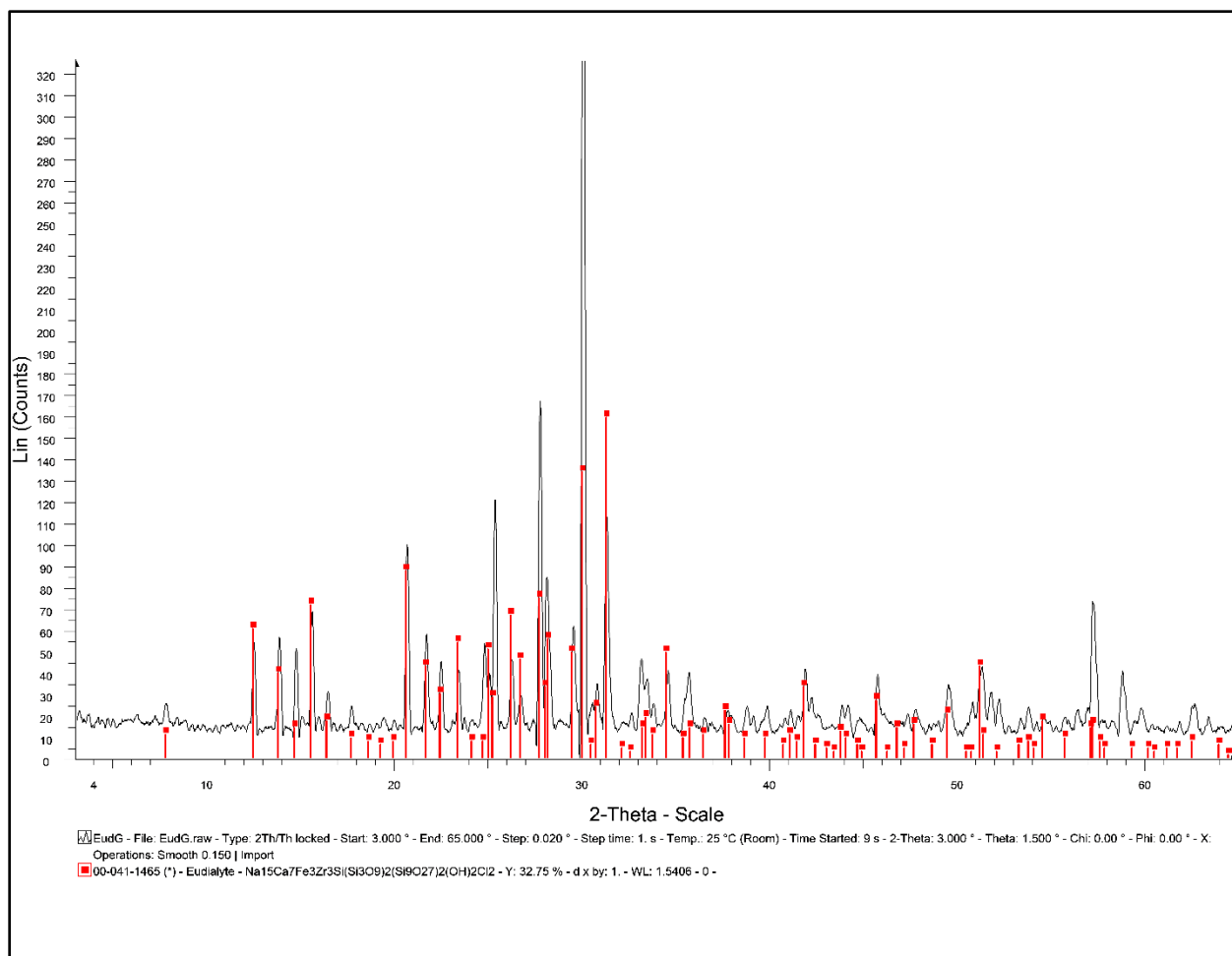
Fig 11: PXRD pattern of eudialyte from Greenland **(G)**
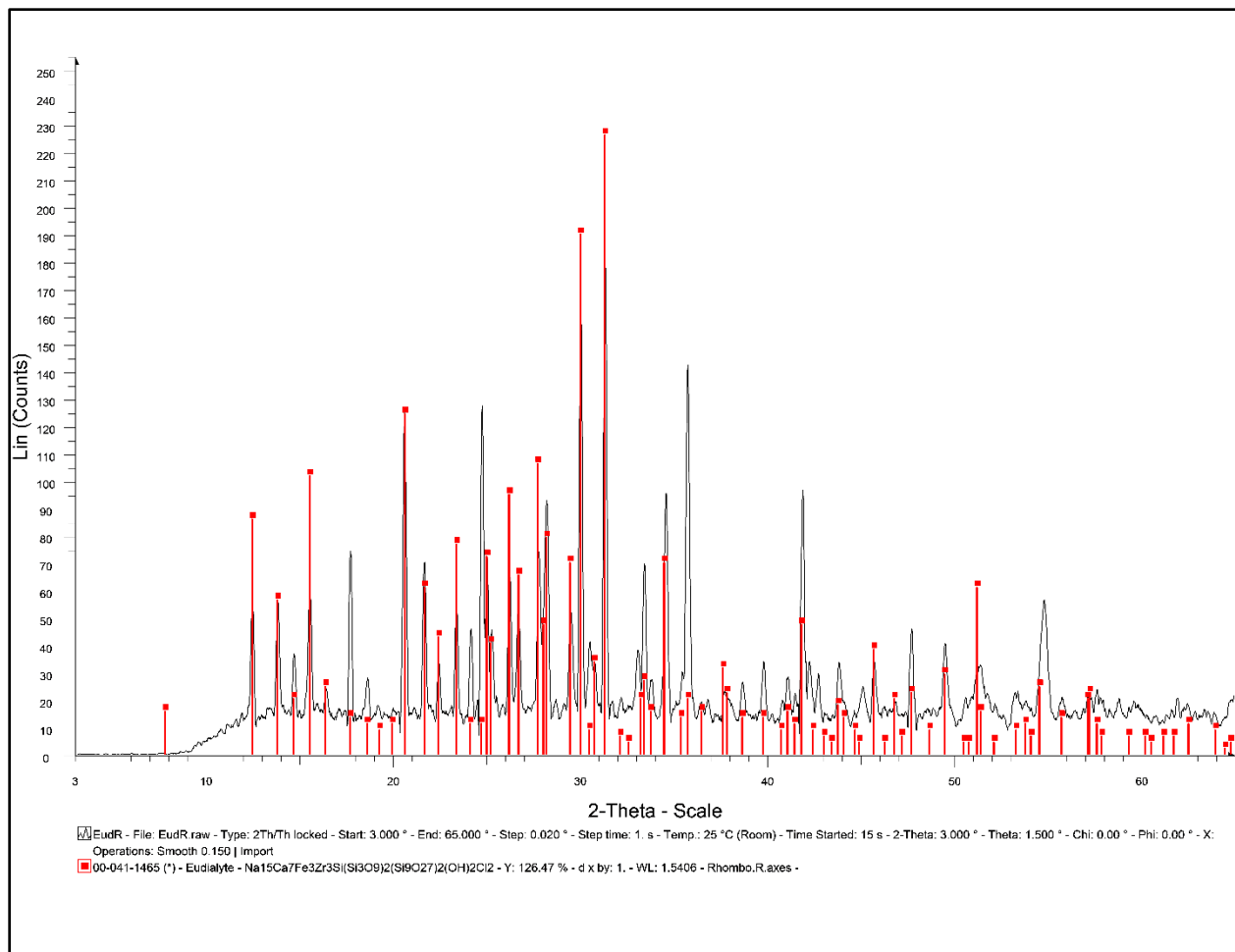
Fig. 12: PXRD pattern of eudialyte from Russia **(R)**

3.2 Analyses in microscale (SEM-EDS)

The theoretical eudialyte EDS spectrum is shown in **Fig. 13**(modified afterSeverin 2004).According to that, the major chemical elements of the mineral are Si, Ca, Zr, Fe, Na, and Cl; the peaks of REE (La-Lu, e.g. Ce and Nd), as well as other minor -or trace- elements (including actinides, i.e. U, Th) have been theoretically indicated.

Eudialyte (Eucolite) $(Na,Ca,Fe)_6Zr[(Si_3O_9)_2](OH,F,Cl)$
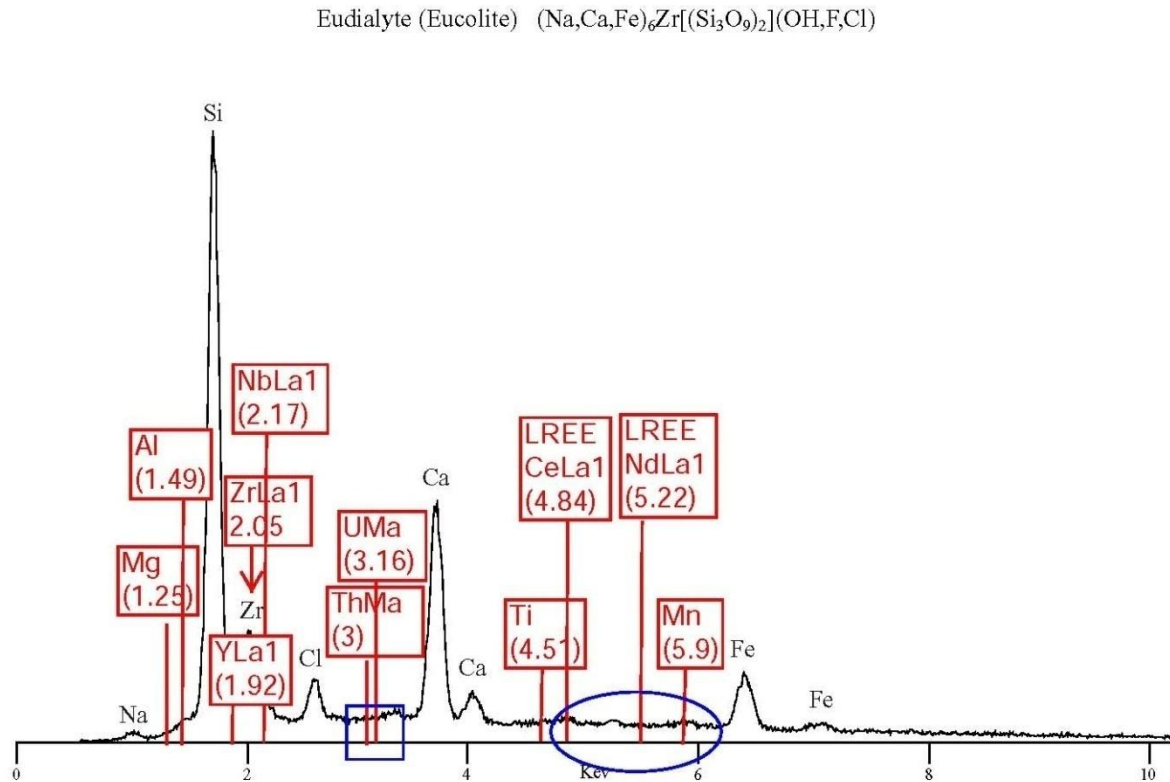
Fig.13: Theoretical eudialyte EDS spectrum (modified after Severin 2004)

Representative data obtained by SEM-EDS, concerning the eudialyte from Russia (R), are shown in **Fig. 14.** It is evident that the major composition of this eudialyte is as expected. However, there are microscopic inclusions of zircon ($ZrSiO_4$) and pyrite (FeS_2). That means, that most of the REE and actinides of the sample -see Section 3.4 below- are presumably contained in eudialyte and some quantities must be hosted in zircon (e.g. Hanchar and

Hoskin 2003). On the other hand, pyrite may host several trace elements like Ni and Co. Besides, there must be a contribution to the Mössbauer spectra (see next Section).
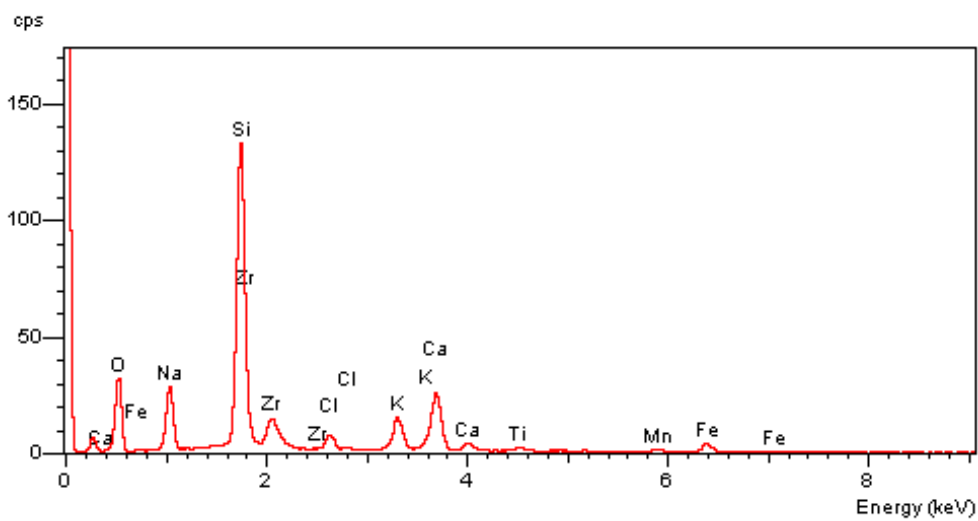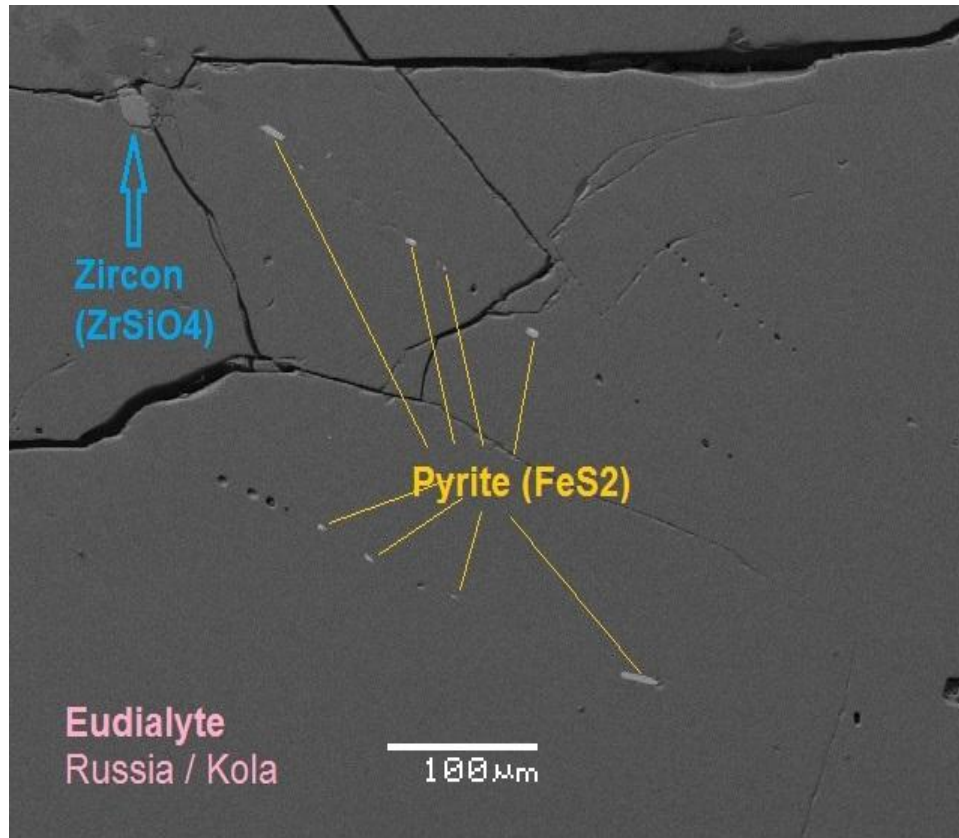
Fig. 14: Representative data obtained by SEM-EDS, concerning the eudialyte from Russia (R)

Representative data obtained by SEM-EDS, concerning the eudialyte from Greenland (G), are shown in **Fig. 15.**According to our data, the major composition of this eudialyte is also as expected, but, in contrast to the Russian sample, there are various types of inclusionscorresponding predominantly to Si-P-REE-Th-(Ca) phases. In general, typical minerals associated with eudialyte include aegirine and arfvedsonite,various Na-Al-silicates such as alkali feldspar,nepheline, sodalite, locally occurring zeolites, anda large number of rare HFSE- and Large IonLithophile Elements (LILE; such as Li, B, Be, Na,Sr)-incorporating minerals, such as astrophylliteandlamprophyllite-group minerals, tugtupite andminerals of the wöhlerite, rosenbuschite andrinkite groups.Specifically, some minor phases constitute a variety of finely disseminated alteration products, which have been also observed by previous authors (e.g. Shilling et al. 2011; Borst et al. 2017; Marks et al. 2020). That means, REE and actinides (see Section 3.4 below) occur, except eudialyte, in various minerals. In addition, it is evident from the present SEM-EDS study that some secondary phases are exceptionally enriched in REE. The exact identification of these minerals needs further micro- and/or nano-analytical work.
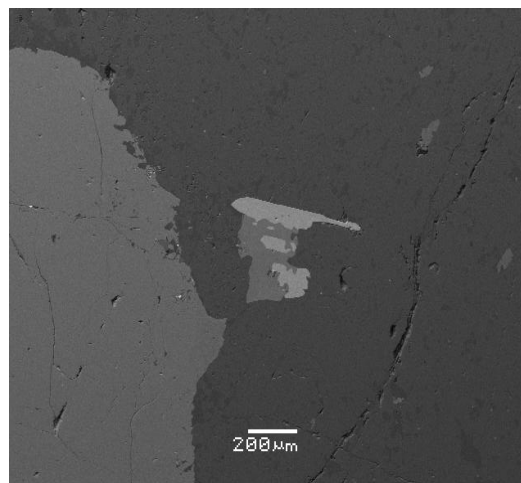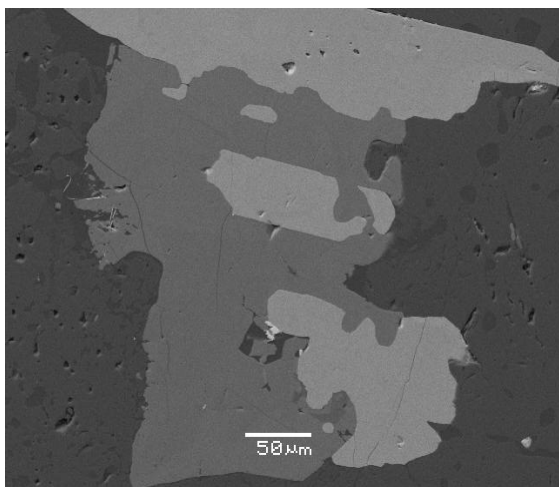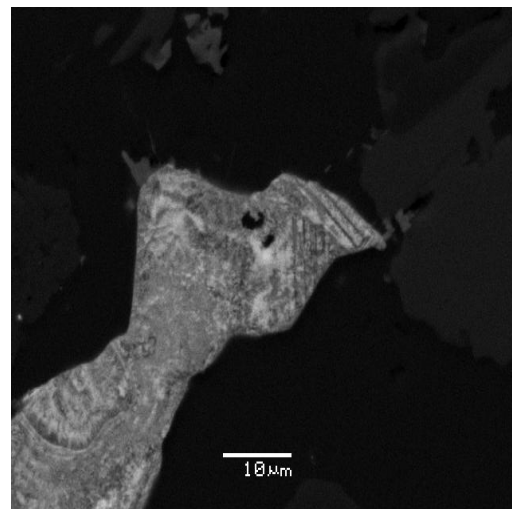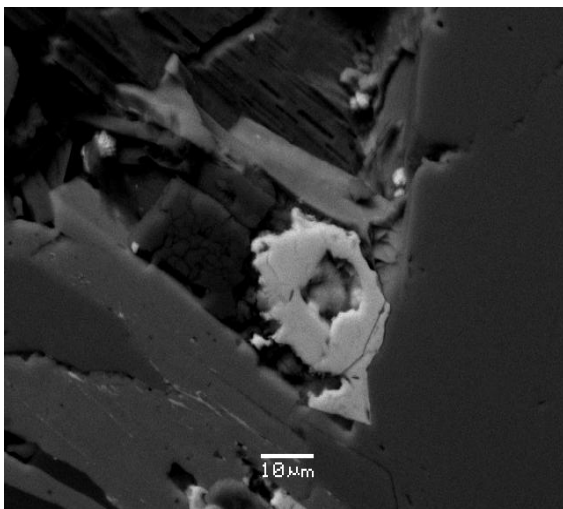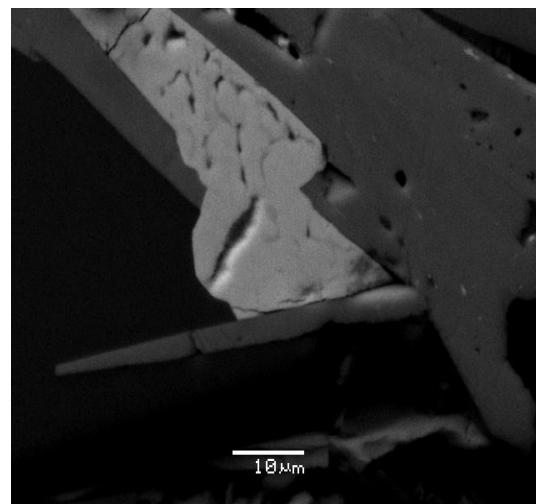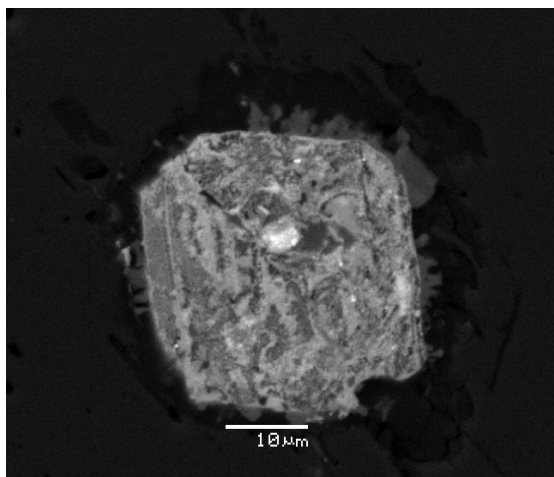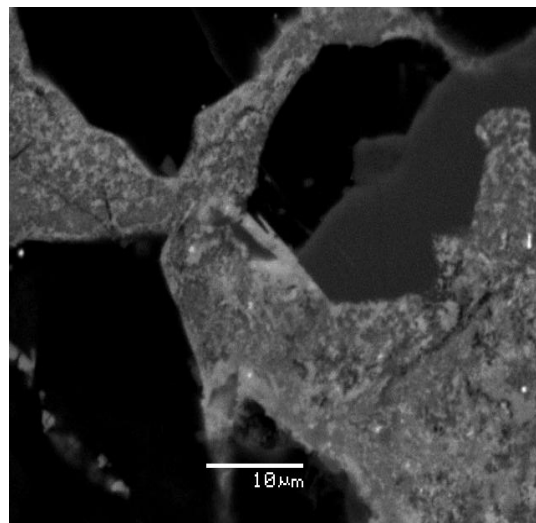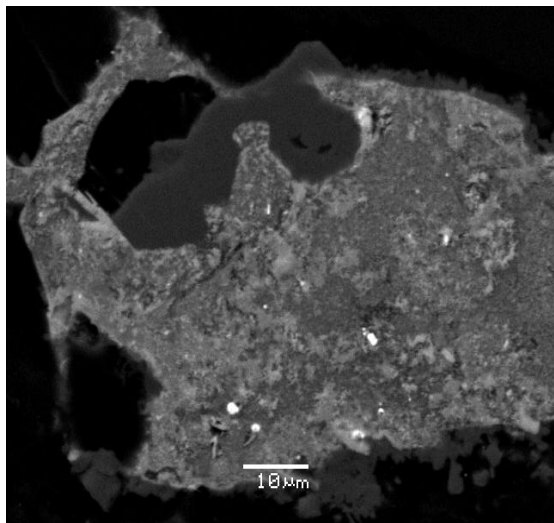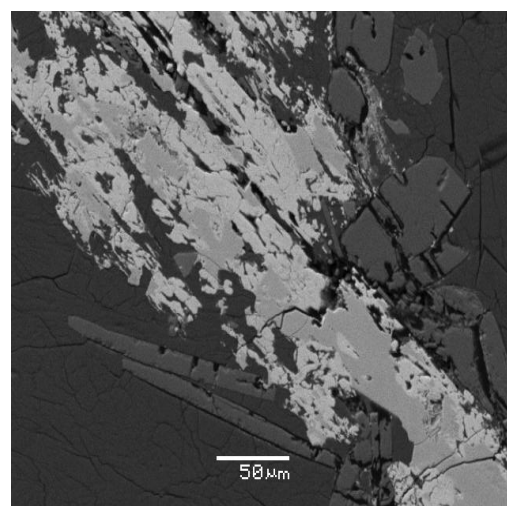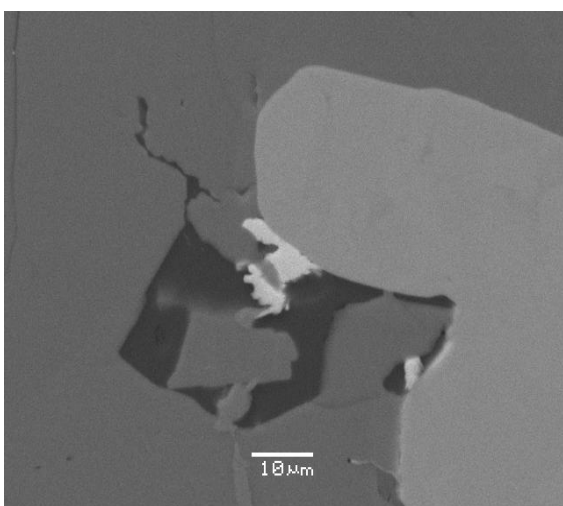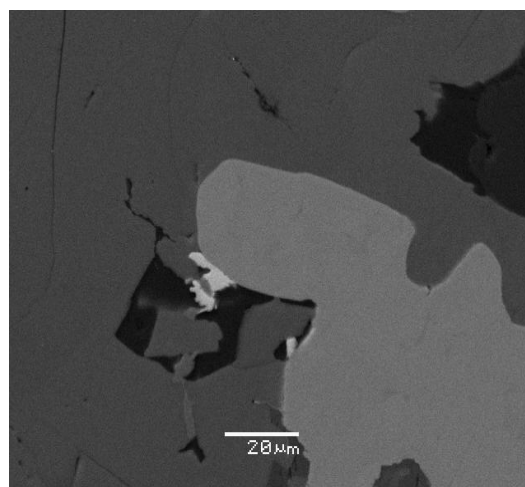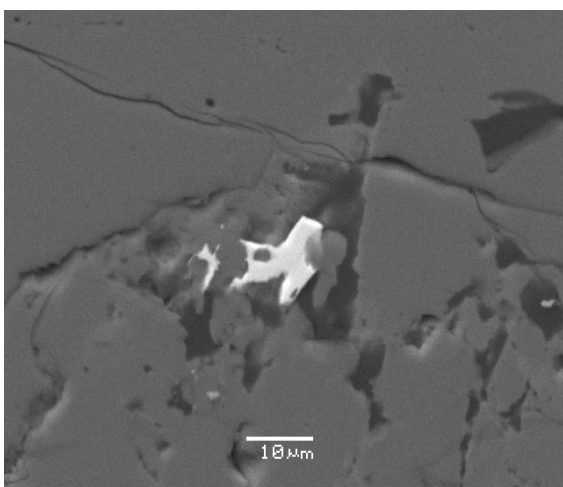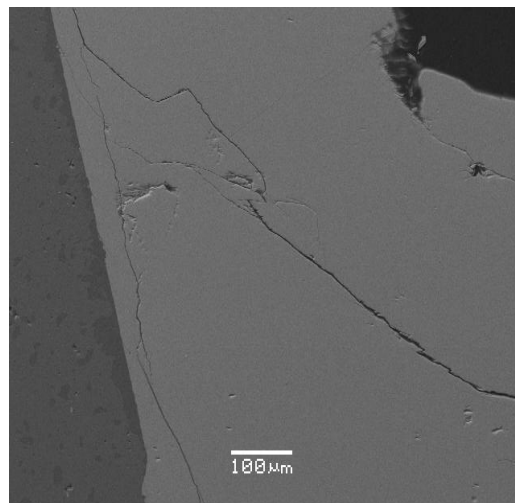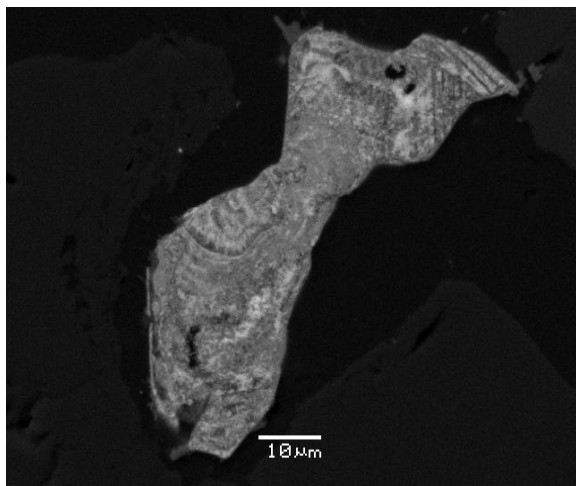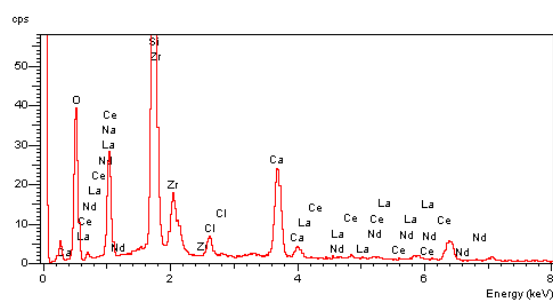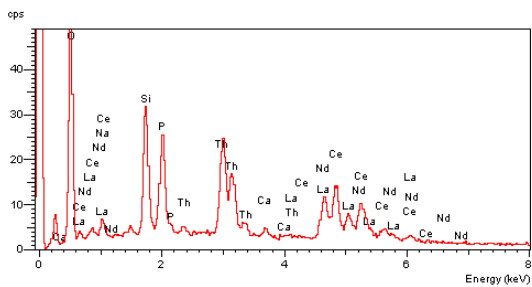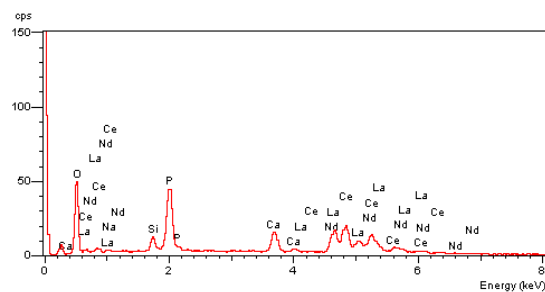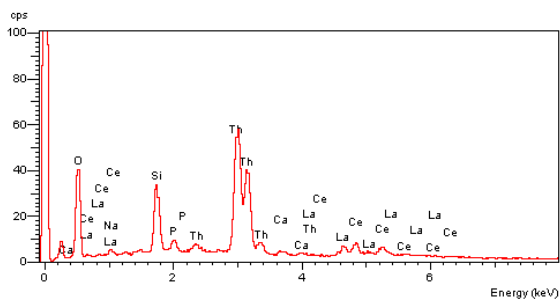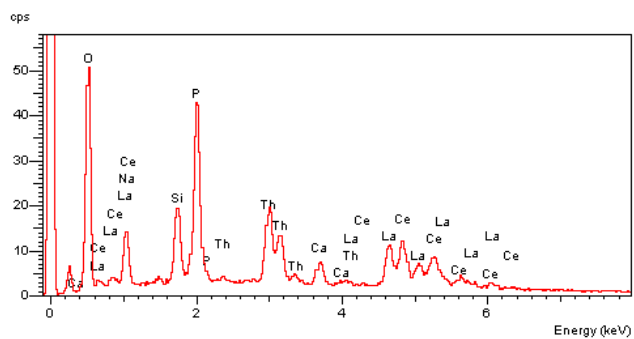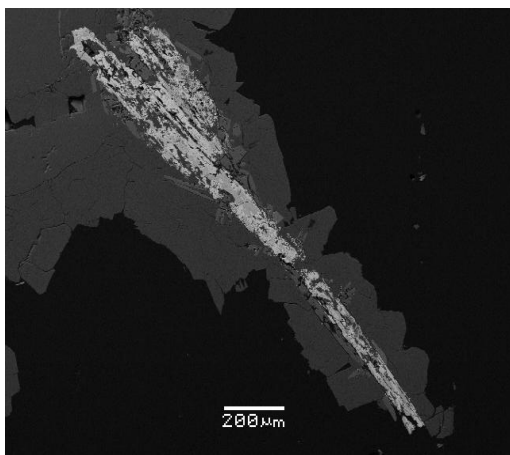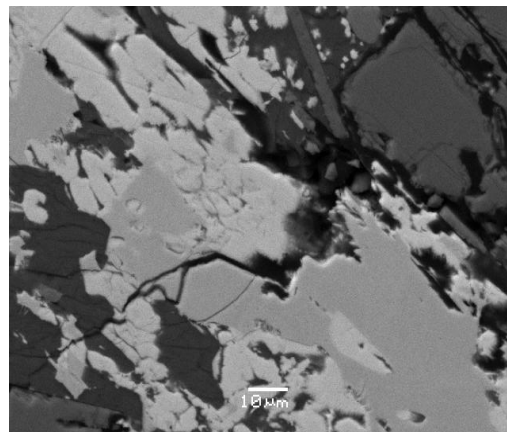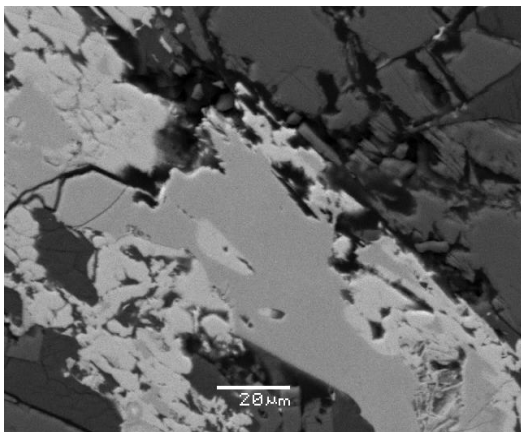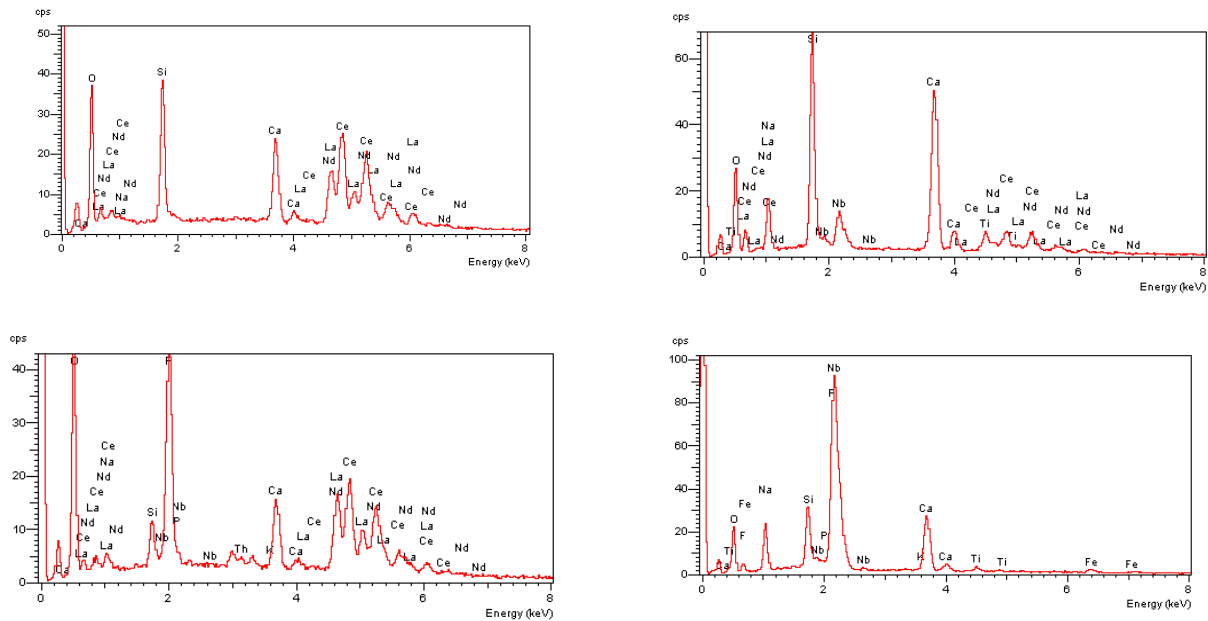
Fig. 15: Representative data obtained by SEM-EDS, concerning the eudialyte from Greenland (G)

3.3. Mössbauer spectroscopic results

Representative Mössbauer spectroscopic results, concerning the eudialyte sample from Russia (R), are shown in **Fig. 16.** The room temperature spectrum of sample R is composed of quadrupole only split contributions. The main contribution comes from an asymmetric doublet (red) corresponding to Fe^{2+}(IV) ions in planar quadrangles, which is the characteristic sign of the typical eudialyte-type minerals (Khomyakov et al. 2010; Schilling et al. 2011; Rastsvetaeva et al. 2020). A second contribution from a symmetric doublet (blue) is attributed to Fe^{2+}(V) ions in square pyramids, also very frequently reported for eudialyte samples. The presence of a minor doublet with Mössbauer parameters characteristic of pyrite (FeS_2; magenta) is included in the fitting model to account for the absorption contribution around 0 mm/s, as well as for the detection of this phase in the SEM images. The presence of an additional component corresponding to Fe^{3+}(VI) ions in octahedral oxygen coordination could be included in the fitting model (fit 1), but in this

case the resulting Mössbauer parameters are shifted relative to those reported in the literature for this Fe^{3+}(VI), as well as for the Fe^{2+}(V) component. Thus the most reliable fitting model is that excluding the Fe^{3+}(VI) component (fit 2).

fit1

IS (mm/s)	QS (mm/s)	Area (%)	Site-Phase	Color
0.80	0.32	79	Fe^{2+}(IV)planarquadrangles	Red
1.25	2.00	10	Fe^{2+}(V)square pyramids	Blue
0.15	0.59	6	Fe^{3+}(VI) octahedra	Green
0.32	0.62	5	FeS_2	Magenta

IS (mm/s)	QS (mm/s)	Area (%)	Site-Phase	Color
0.81	0.35	83	Fe^{2+}(IV) planar quadrangles	Red
1.11	2.28	10	Fe^{2+}(V) square pyramids	Blue
0.32	0.62	7	FeS_2	Magenta
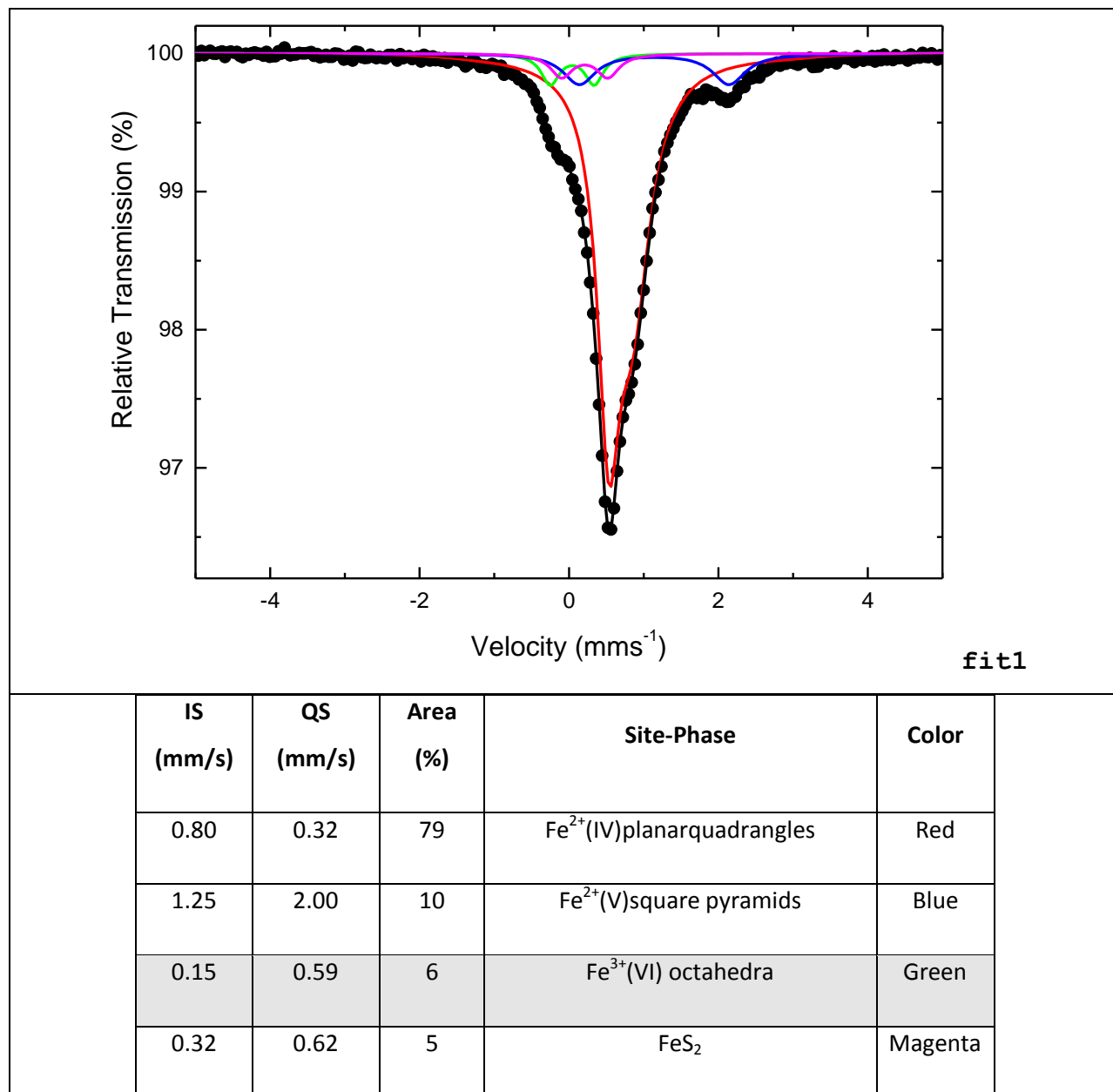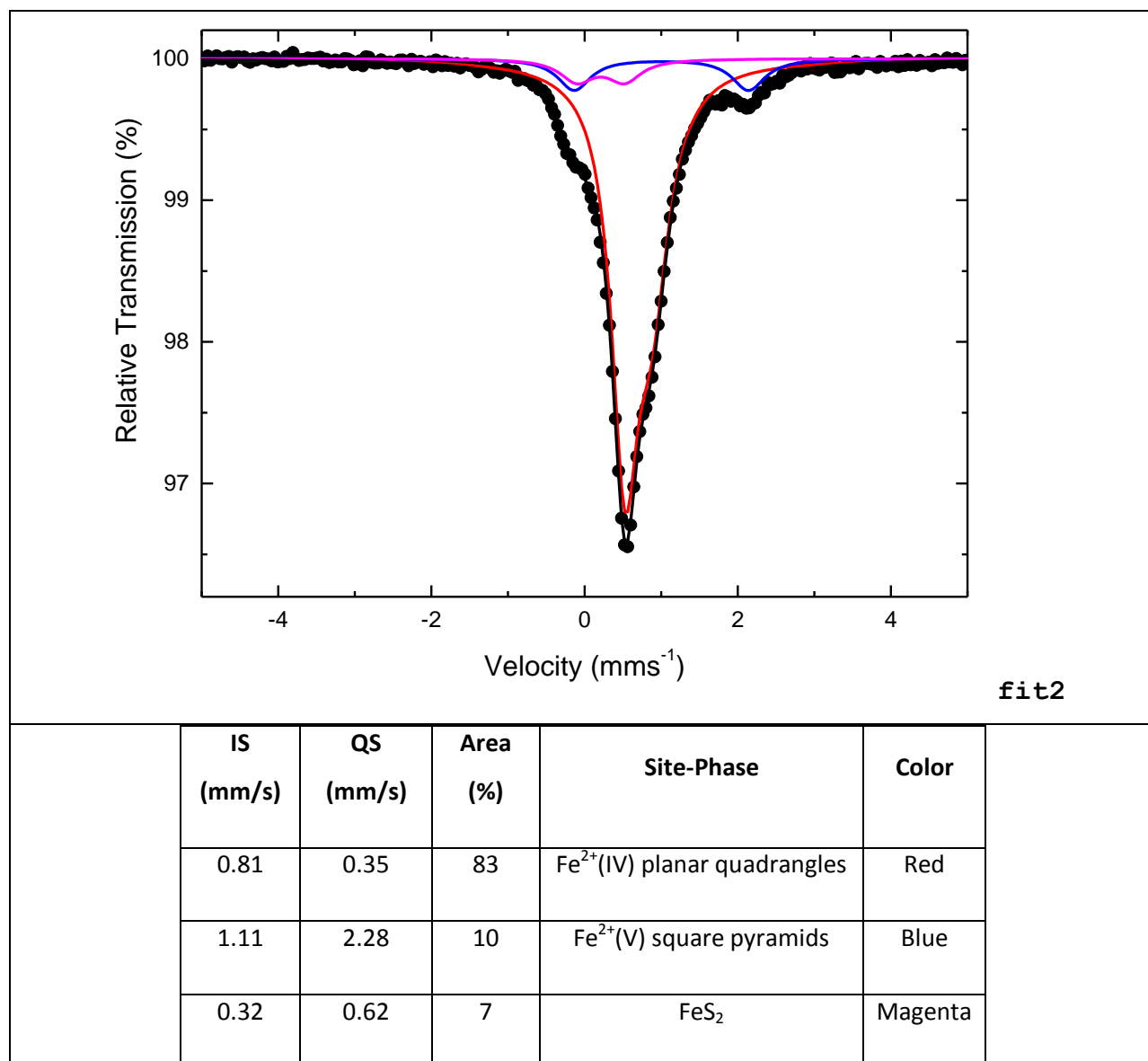
Fig. 16: Mossbauer spectroscopic results of eudialyte(Russia)

3.4. Mineral chemistry & geochemistry

The bulk analytical results, concerning eudialyte crystals, are presented in **Tables 1-2** and **Figs. 17-20.** According to the results of the Upper Continental Crust (UCC)-normalized multielement and lanthanides-actinides spider diagrams (see **Fig.17** and **Fig.18**), there is an enrichment to the majority of the HFSE and LILE elements in both samples. The Greenland sample (G) contains , in general, higher concentrations of REE (see **Table 2.**). On the other hand, the actinide (U, Th) content is increased in the case of the examined eudialyte from Russia (R), related to relatively higher natural radioactivity (see Section 3.5). Regarding REE geochemical anomalies (see **Figs. 19-20**), it is evident that eudialyte from Greenland (G) is totally different, exhibiting a crucial negative Eu (Eu/Eu*) anomaly.

Table 1: Bulk analyses of eudialyte crystals from Greenland (G) and Russia (R)

	Eudialyte Greenland (G)	Eudialyte Russia (R)	
	wt.%	wt.%	
SiO2	51.54	52	
ZrO2	*	*	*>5 wt.%
Al2O3	0.38	0.05	
Fe2O3	6.51	5.47	
MgO	0.02	0.02	
CaO	10.67	11.36	
Na2O	14.6	14.32	
K2O	0.29	2.85	
TiO2	0.05	0.6	
P2O5	0.02	0.03	
MnO	0.75	0.54	
Cr2O3	0.009	0.002	
TOT/C	0.05	0.02	
TOT/S	0.01	0.03	
OH, H2O	*	*	n.a.

	ppm	ppm	
Ce	7037.5	924.5	
Y	5211.3	1349.8	
La	3699.5	421.1	
Nd	3006.5	477	
Hf	2071.6	1336.6	
Nb	1001	1001	>0.1 wt.%
Dy	994.84	240.15	
Pr	799.81	114.06	
Er	768.41	167.05	
Gd	738.29	186.29	
Yb	713.69	133.15	
Sm	659.21	134.41	
Ta	614.3	177.4	
Ho	239.01	54.81	
W	193.7	68.2	
Zn	160	11	
Tb	147.17	36.65	
Pb	128.2	24.9	
Tm	117.44	23.57	
Sn	105	49	
Lu	99.24	17.15	
Sr	91.3	7495.4	
Eu	63.43	50.85	
U	62.2	83.4	
Se	37.6	8.4	
Rb	34.6	26	
Th	32.1	28.7	
Cd	28	24.8	
V	21	55	
Cu	19.1	1.8	
Ba	13	1341	
Mo	9.2	2.8	
Be	4	0.5	
Cs	2	0.6	
Ni	1.9	0.9	
Ga	0.9	0.25	
Au	0.5096	0.3347	
Sc	0.5	0.5	
Tl	0.5	0.05	
Sb	0.4	0.4	
As	0.25	0.25	
Hg	0.22	0.01	
Bi	0.2	0.05	
Co	0.1	0.7	
Ag	0.05	0.5	

Table 2 : Analytical results concerning REE

	Eudialyte Greenland (G)	Eudialyte Russia (R)
	ppm	ppm
La	3699.5	421.1
Ce	7037.5	924.5
Pr	799.81	114.06
Nd	3006.5	477
Sm	659.21	134.41
Eu	63.43	50.85
Gd	738.29	186.29
Tb	147.17	36.65
Dy	994.84	240.15
Ho	239.01	54.81
Er	768.41	167.05
Tm	117.44	23.57
Yb	713.69	133.15
Lu	99.24	17.15
	ppm	ppm
ΣREE	19084.04	2980.74
	wt.%	wt.%
ΣREE	1.91	0.30
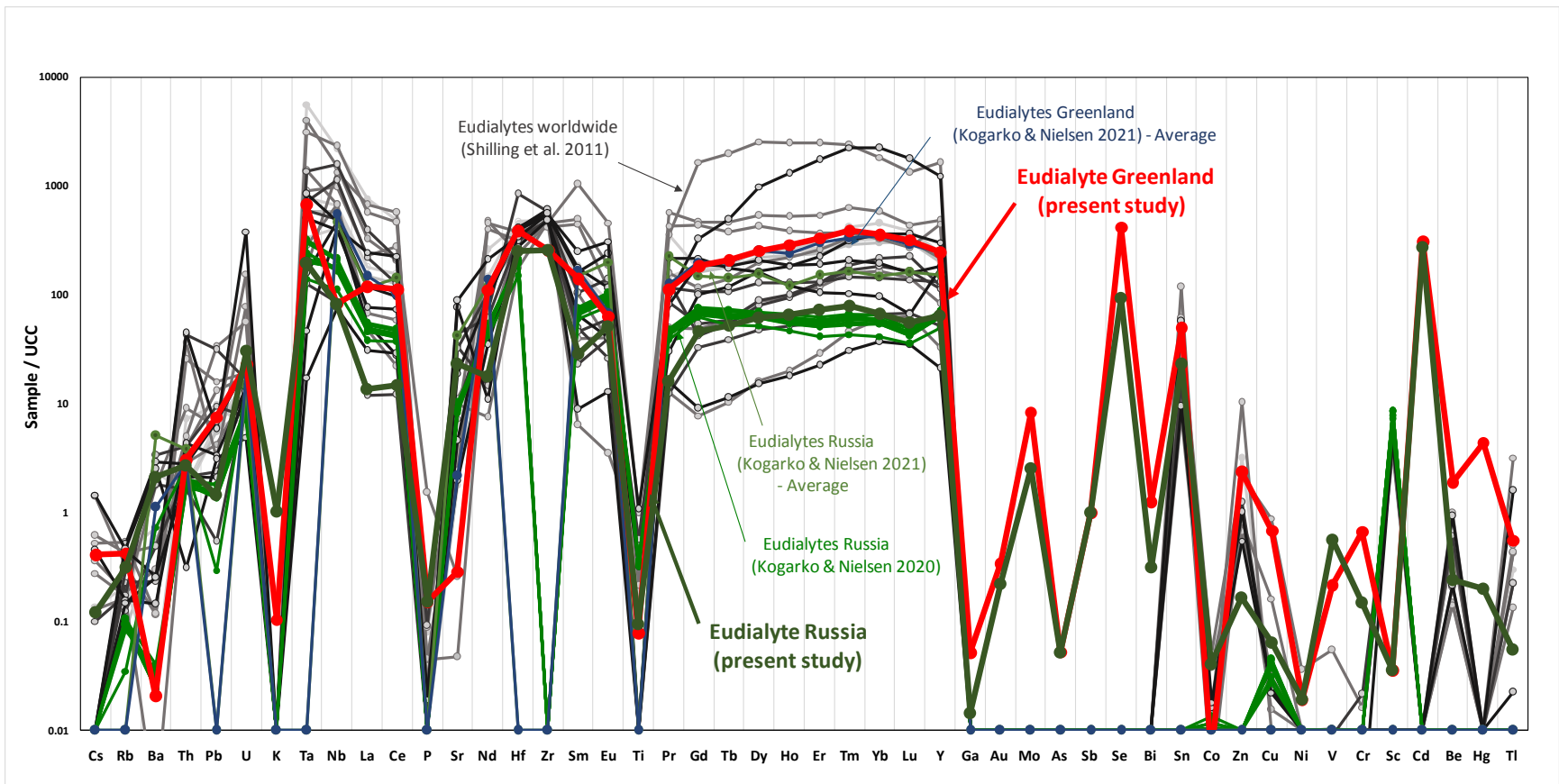
Fig.17: Upper Continental Crust (UCC)-normalized (Rudnick and Gao, 2003) multielement spider diagram for the studied eudialyte crystals from Greenland and Russia in comparison with data in the literature (Shilling et al. 2011; Kogarko and Nielsen 2020 & 2021)
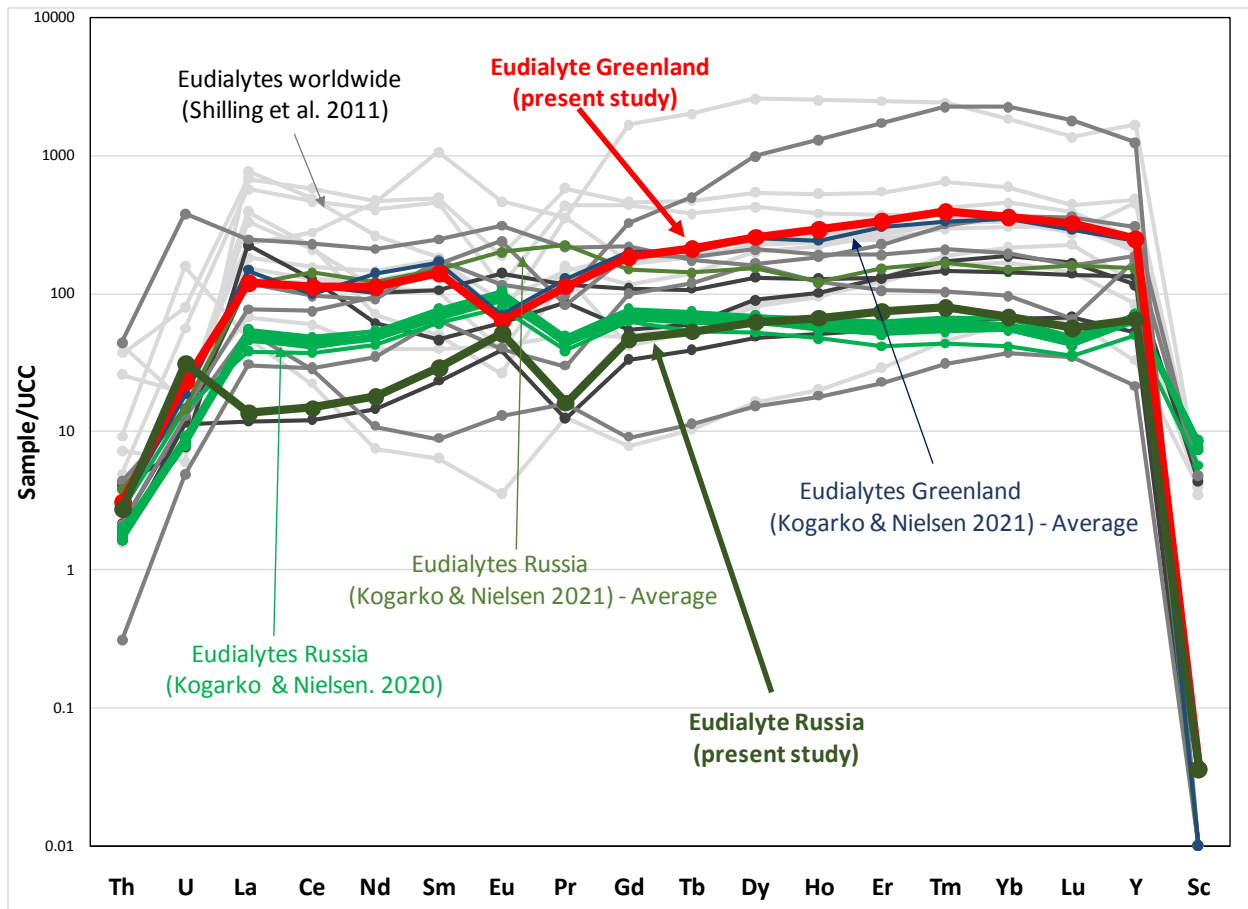
Fig.18: Upper Continental Crust (UCC)-normalized (Rudnick and Gao, 2003) multielement spider diagram for actinides (U, Th) & lanthanides (REE+Y+Sc) concerning the studied eudialyte crystals from Greenland and Russia in comparison with data in the literature (Shilling et al. 2011; Kogarko and Nielsen 2020 & 2021)
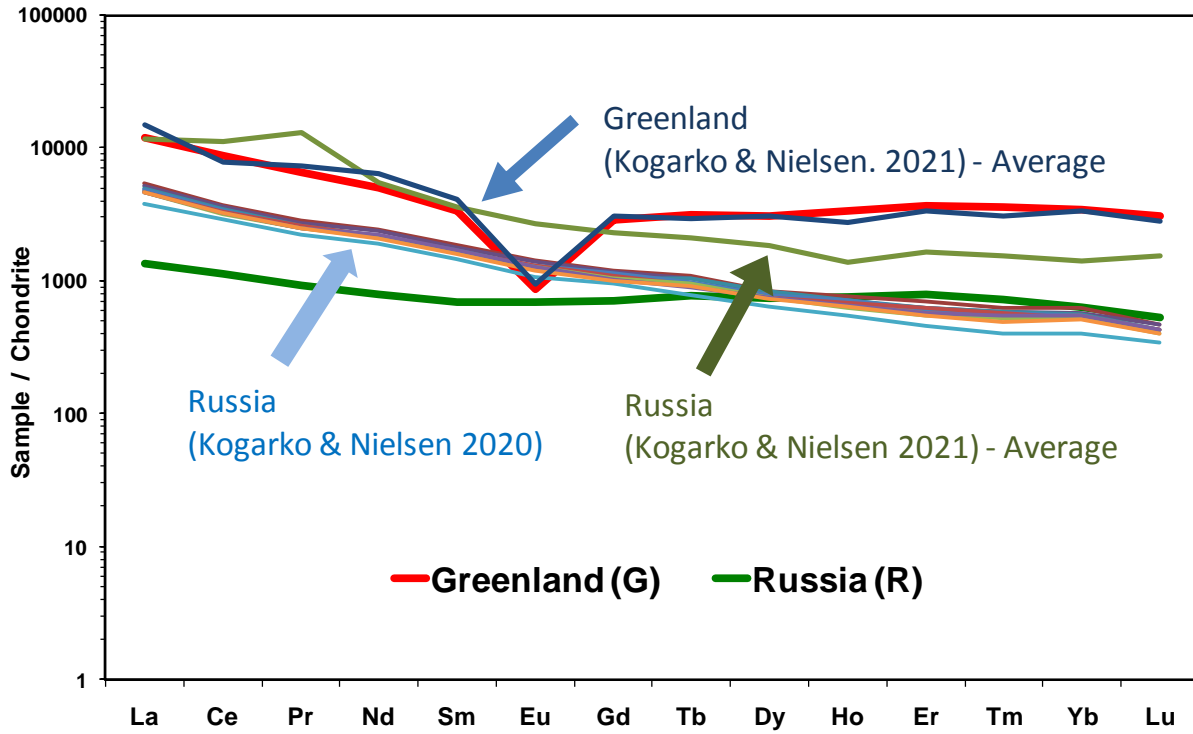
Fig.19: Chondrite-normalized (McDonough and Sun, 1995) REE patterns for the studied eudialyte crystals from Greenland and Russia in comparison with data in the literature (Shilling et al. 2011; Kogarko and Nielsen 2020 & 2021)
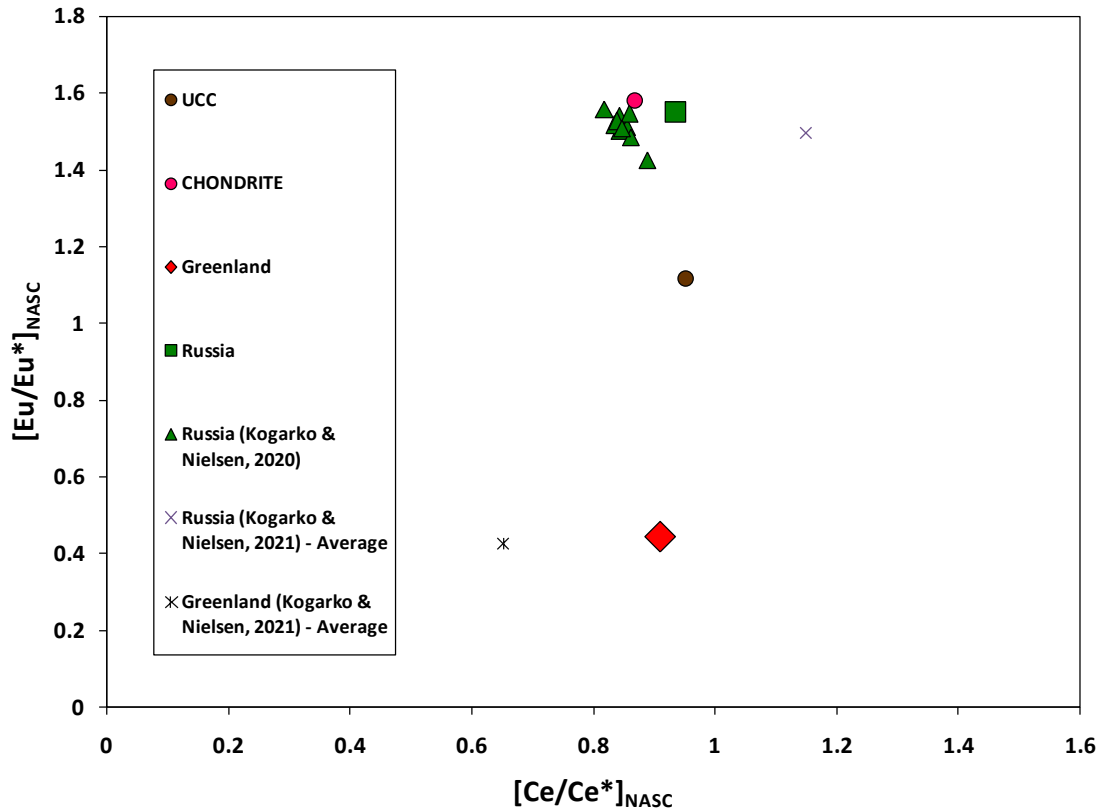
Fig.20: Binary correlation diagram of Eu *vs* Ce anomalies (normalized to NASC; Gromet et al., 1984) for the studied eudialyte crystals from Greenland and Russia. Europium anomalies calculated as: Eu/Eu* = 2(Eu/EuNASC)/({Sm/SmNASC)+(Gd/GdNASC)} from Liu et al. (2013). Cerium anomalies calculated as: Ce/Ce* = 3(Ce/CeNASC)/({2 La/LaNASC)+(Nd/NdNASC)} after German and Elderfield (1990).

3.5 Gamma-ray spectrometry

The data obtained by γ-ray spectrometry concerning the eudialyte from Russia (R) and eudialyte from Greenland (G) are shown in **Figs. 21–23 and Table 3.** It is obvious that significant amounts of natural radionuclides (U- and Th-series) are present in the samples, which in turn indicates that U and Th, detected ICP-OES/MS analyses (see section 3.4), are indeed concentrated in eudialyte . The eudialyte from Russia seems to be more radioactive (see **Fig.23**and **Table.3**), due to the fact that contains more U than the one from Greenland. It also contains significant amounts of ^{40}K (also natural radioactivity), in contrast with Greenland sample that not. Also, the eudialyte from Russia contains measurable quantity of ^{137}Cs, possibly due to 'contamination' of the outcrop by the Chernobyl disaster. Of course, the sample from Greenland is free of artificial/anthropogenic radionuclides.
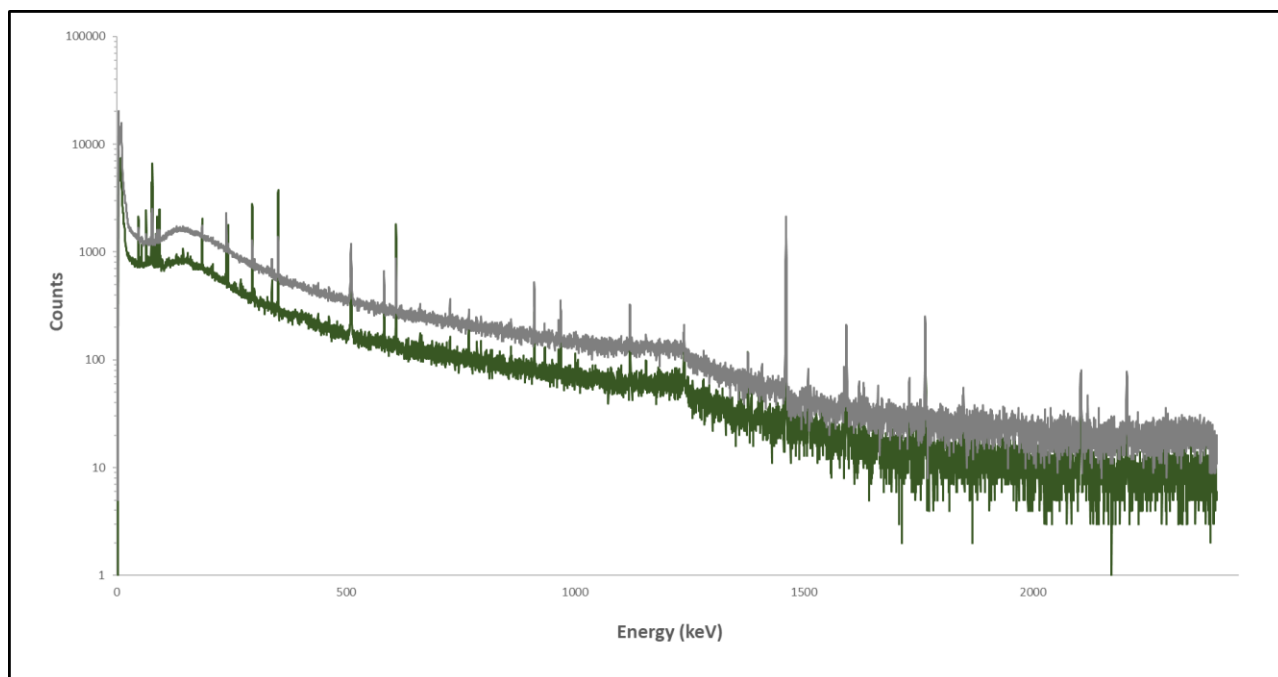
Fig. 21: γ-ray spectrum of eudialyte from Russia**(R)**(Green : sample , Grey : backround)
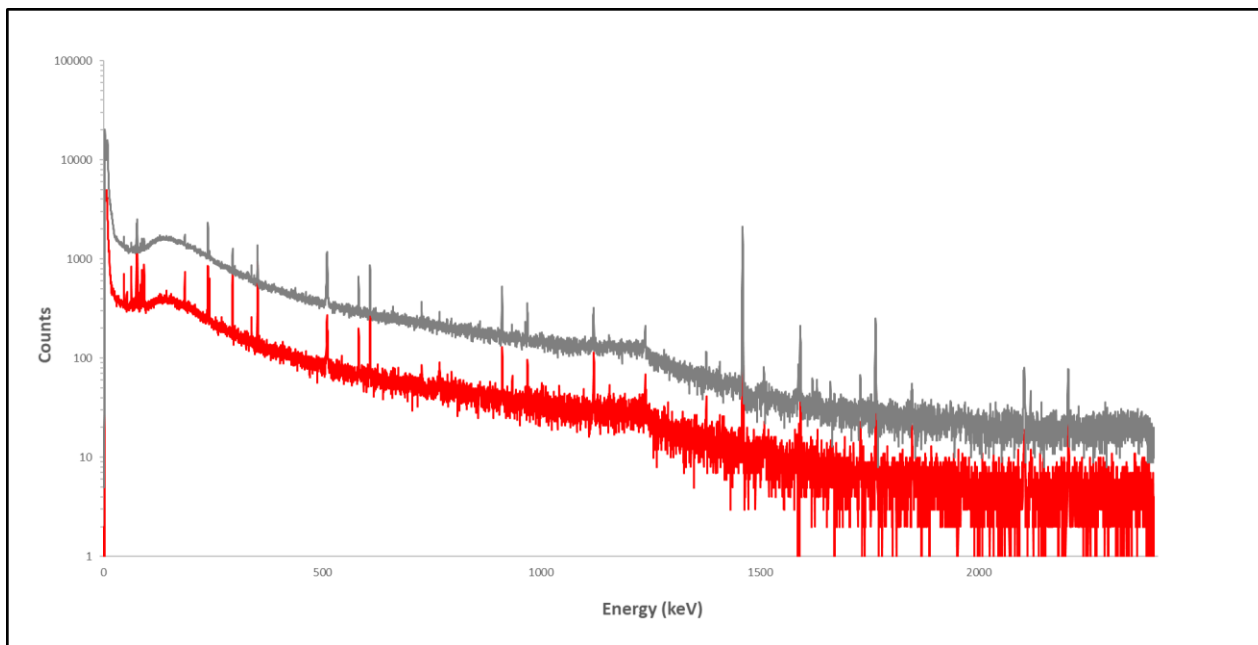
Fig.22: γ-ray spectrum of eudialyte from Greenland **(G)** (Red : sample , Grey : backround)
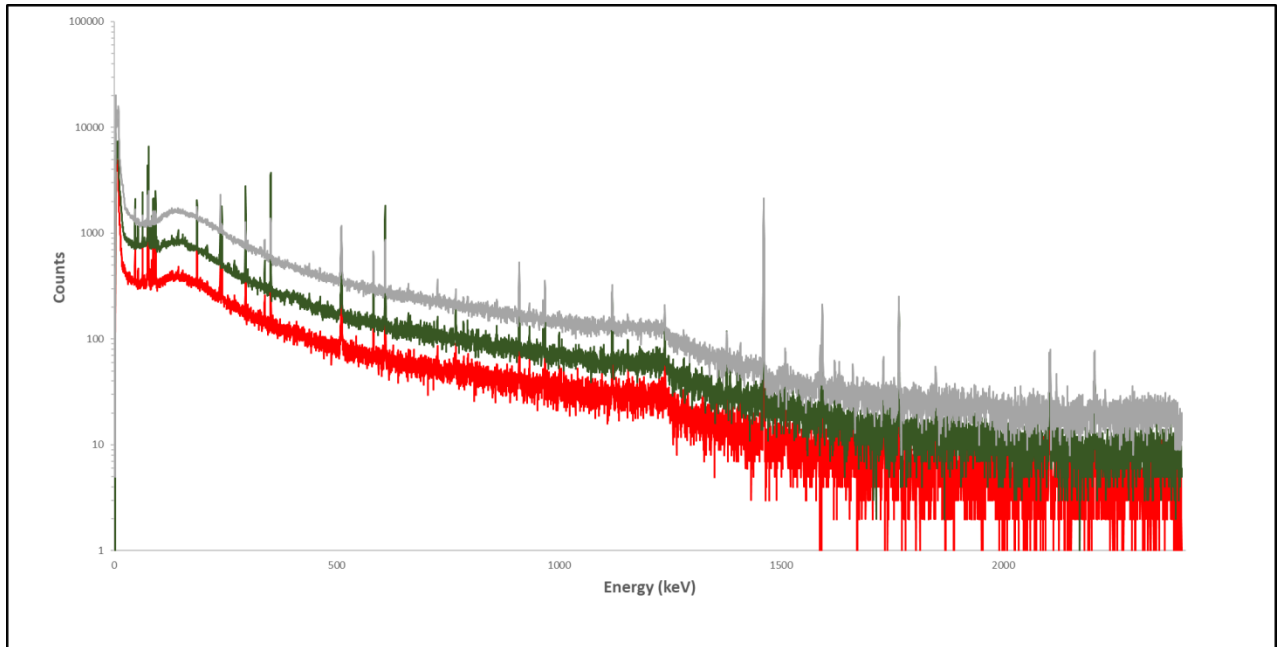
Fig.23: Comparison of γ-ray spectra of **R** and **G.**

Table 3: γ-ray spectroscopic results

backgroundtime 789501 background dec21v2

Nuclide	Energy	Area	±	Area Interference Correction	Cps	background dec21v2	±	BG/s	Net c/s	±	Efficiency, 260 ml,	efficiency ±	FY	Branching Correction	Bq/Kg	±	MDA
Th-234	63.5	1268.27	88	1245.44114	0.00738547	487	112.01	0.00061685	0.0067686	0.0005408	0.118478487	0.011847849	0.039	0	853	85	0.50
Pa-234	1001	51	23.97		0.00030243	87	49.59	0.0001102	0.0001922	0.0001554	0.012676068	0.001267607	0.01021	0	865	87	7.00
Ra-226 Gilmore corection	186.2	1530.87	114	874.12677	0.00518357	1372	150.92	0.00173781	0.0034458	0.0007025	0.109994818	0.010999482	0.03533	0	516	52	0.80
Ra-226 ftom 143 keV	186.2	1530.87	114	911.4795826	0.00540508	1372	150.92	0.00173781	0.0036673	0.0007025	0.109994818	0.010999482	0.03533	0	550	55	
Ra-226 from Th-234	186.2	1530.87	114	807.9817174	0.00479133	1372	150.92	0.00173781	0.0030535	0.0007025	0.109994818	0.010999482	0.03533	0	458	46	
Ra-226 from Pa-234	186.2	1530.87	114	797.8857201	0.00473146	1372	150.92	0.00173781	0.0029937	0.0007025	0.109994818	0.010999482	0.03533	0	449	45	
Ra-226 from average Pa-234 Th-234	186.2	1530.87	114	802.9337188	0.0047614	1372	150.92	0.00173781	0.0030236	0.0007025	0.109994818	0.010999482	0.03533	0	453	45	
Pb-214	352	3775	97		0.02238576	2940	163	0.00372387	0.0186619	0.0006111	0.04673879	0.004673879	0.3534	0	658	66	0.15
Bi-214	609.3	2393.18	73		0.01419156	2532	126	0.00320709	0.0109845	0.0004614	0.02223655	0.002223655	0.4516	0	637	64	0.20
Bi-214	1764	480.18	30		0.00284747	1461	56	0.00185054	0.0009969	0.0001915	0.006850222	0.000685022	0.1531	0	554	55	1.20
U-235	144	225	67.5	156.825	0.00092997	53	53	6.7131E-05	0.0008628	0.0004059	0.134855739	0.013485574	0.1096	0	34	3	0.20
	163.5	0	0	0	0	10	10	1.2666E-05	-1.27E-05	1.267E-05	0.123385259	0.012338526	0.0508	0	-1	0	0.50
	186	1530.87	114	655.21236	0.00388541	1372	150.92	0.00173781	0.0021476	0.0007025	0.109994818	0.010999482	0.572	0	20	2	0.05
Ac-228	911	448	46		0.00265664	1738	100	0.00220139	0.0004553	0.0003008	0.014013284	0.001401328	0.258	0	73	7	0.40
Pb-212	238.6	1854.83	58		0.01099915	3661	178	0.00463711	0.006362	0.0004112	0.079494334	0.007949433	0.436	0	107	11	0.08
Bi-212	727.3	102	49	93.432	0.00055405	392	70.56	0.00049652	5.754E-05	0.000304	0.018131515	0.001813152	0.0674	0	27	3	1.10
Tl-208	583.1	537.45	56		0.00318708	1710	112	0.00216593	0.0010212	0.0003611	0.023381696	0.00233817	0.845	30.10152587	84	3	0.10
K-40	1461	2830.51	59		0.01678493	13256	129	0.01679035	-5.42E-06	0.0003861	0.008520838	0.000852084	0.1066	0	-3	0	3.50
Cs-137	661.6	0	0		0	83	73.04	0.00010513	-0.000105	9.251E-05	0.020232833	0.002023283	0.851	0	-3.56	0.36	0.10

Eudialyte Russia

backgroundtime 789501 background dec21v2

Nuclide	Energy	Area	±	Area Interference Correction	Cps	background dec21v2	±	BG/s	Net c/s	±	Efficiency, 260 ml,	efficiency ±	FY	Branching Correction	Bq/Kg	±	MDA
Th-234	63.5	4053.7	137	3980.7334	0.01205695	487	112.01	0.00061685	0.0114401	0.0004385	0.105971101	0.01059711	0.039	0	1251	125	0.50
Pa-234	1001	150	30		0.00045432	87	49.59	0.0001102	0.0003441	0.0001105	0.012555645	0.001255564	0.01021	0	1213	121	7.00
Ra-226 Gilmore corection	186.2	5218.17	172	2979.57507	0.00902461	1372	150.92	0.00173781	0.0072868	0.0005549	0.107579378	0.010757938	0.03533	0	866	87	0.80
Ra-226 ftom 143 keV	186.2	5218.17	172	2579.64308	0.00781329	1372	150.92	0.00173781	0.0060755	0.0005549	0.107579378	0.010757938	0.03533	0	722	72	
Ra-226 from Th-234	186.2	5218.17	172	2602.456547	0.00788239	1372	150.92	0.00173781	0.0061446	0.0005549	0.107579378	0.010757938	0.03533	0	731	73	
Ra-226 from Pa-234	186.2	5218.17	172	2681.481605	0.00812174	1372	150.92	0.00173781	0.0063839	0.0005549	0.107579378	0.010757938	0.03533	0	759	76	
Ra-226 from average Pa-234 Th-234	186.2	5218.17	172	2641.969076	0.00800206	1372	150.92	0.00173781	0.0062643	0.0005549	0.107579378	0.010757938	0.03533	0	745	74	
Pb-214	352	12431.71	155		0.03765348	2940	163	0.00372387	0.0339296	0.0005129	0.045986872	0.004598687	0.3534	0	943	94	0.15
Bi-214	609.3	7477.79	117		0.02264892	2532	126	0.00320709	0.0194418	0.0003887	0.02195715	0.002195715	0.4516	0	886	89	0.20
Bi-214	1764	1348.79	47		0.00408525	1461	56	0.00185054	0.0022347	0.000159	0.006799617	0.000679962	0.1531	0	970	97	1.20
U-235	144	912.35	159	635.90795	0.00192605	53	53	6.7131E-05	0.0018589	0.0004862	0.130599095	0.01305991	0.1096	0	59	6	0.20
	163.5	0	0	0	0	10	10	1.2666E-05	-1.27E-05	1.267E-05	0.120158764	0.012015876	0.0508	0	-1	0	0.50
	186	5218.17	172	2233.37676	0.00676451	1372	150.92	0.00173781	0.0050267	0.0005549	0.107579378	0.010757938	0.572	0	37	4	0.05
Ac-228	911	1052.65	75		0.00318829	1738	100	0.00220139	0.0009869	0.0002601	0.013873474	0.001387347	0.258	0	125	12	0.40
Pb-212	238.6	4088.97	82		0.01238478	3661	178	0.00463711	0.0077477	0.0003354	0.07811657	0.007811657	0.436	0	103	10	0.08
Bi-212	727.3	227.43	59	208.32588	0.00063098	392	70.56	0.00049652	0.0001345	0.0001998	0.017923319	0.001792332	0.0674	0	50	5	1.10
Tl-208	583.1	1050.49	94		0.00318175	1710	112	0.00216593	0.0010158	0.0003181	0.023082644	0.002308264	0.845	23.53398619	65	2	0.10
K-40	1461	5959.23	16.4		0.01804947	13256	129	0.01679035	0.0012591	0.0001708	0.008450667	0.000845067	0.1066	0	632	63	3.50
Cs-137	661.6	156.54	31		0.00047413	83	73.04	0.00010513	0.000369	0.0001318	0.019988292	0.001998829	0.851	0	9.80	0.98	0.10

	Bq/kg					
	U-238	Ra-226	average(Pb-214, Bi-214)	Th-232 (average(Ac-228, Pb-212)	K-40	Cs-137
EudyliteG	859	453	648	90	0	0
EudyliteR	1232	745	915	114	632	10

References

Borst, A., Finch, A., Friis, H., Horsburgh, N., Gamaletsos, P., Goettlicher, J., Steininger, R., Geraki, K. (2020). Structural state of rare earth elements in eudialyte-group minerals. Mineralogical Magazine, 84(1), 19-34.

Borst, A., Friis, H., Finch, A. (2017) . Optimising the REE-Zr-Nb potential of eudialyte and its alteration products in the Ilímaussaq complex, South Greenland. Applied Earth Science IMM Transactions section B 126(2):1-1

German, C.R., Elderfield, H., (1990). Application of the Ce anomaly as a paleoredox indicator: The ground rules. Paleoceanography 5, 823-833.

Gromet, L.P., Dymek, R.F., Haskin, L.A., Korotev, R.L. (1984). The 'North American shale composite': Its compilation, major and trace element characteristics. Geochim. Cosmochim. Acta 48, 2469-2482.

Goodenough, Kathryn & Schilling, J. & Jonsson, Erik & Kalvig, Per & CHARLES, Nicolas & Tuduri, Johann & Deady, E.A. & Sadeghi, Martiya & Schiellerup, Henrik & Müller, Axel & Bertrand, Guillaume & Arvanitidis, Nikolaos & Eliopoulos, Demetrios & Shaw, Richard & Thrane, Kristine & Keulen, Nynke. (2016). Europe's rare earth element resource potential: An overview of REE metallo- genetic provinces and their geodynamic setting. Ore Geology Reviews. Volume 72, Part 1, Pages 838-856.

Johnsen O., Ferraris G., Gault R.A., Grice J.D., Kampf A.R. and Pekov I.V. (2003) The nomenclature of eudialyte-group minerals. The Canadian Mineralogist, 41, 785–794.

Hanchar, J.M. Hoskin P.W.O. (eds.), (2003). MSA reviews in mineralogy and geochemistry, Washington.

Kogarko, L.; Nielsen, T.F.D. (2020) Chemical Composition and Petrogenetic Implications of Eudialyte-Group Mineral in the Peralkaline Lovozero Complex, Kola Peninsula, Russia. Minerals, 10, 1036.

Kogarko L., Nielsen T.F.D. (2021) Compositional Variation of Eudialyte-Group Minerals

from the Lovozero and Ilímaussaq Complexes and on the Origin of Peralkaline Systems. Minerals, 11, 548.

Khomyakov et al., (2010). Phys. Chem. Minerals, 37:543–554.

Liu X., Wang Q., Feng Y., Li Z. and Cai S. (2013) Genesis of the Guangou karstic bauxite deposit in western Henan, China. Ore Geol. Rev. 55, 162-185.

Marks, M.A., Eggenkamp, H.G., Atanasova P., Mundel F., Kümmel S., Hagen M., Wenzel T. and Markl, G. (2020). Review on the Compositional Variation of Eudialyte-Group Minerals in the Ilímaussaq Complex (South Greenland). Minerals, 10(11), p.1011

Mc Donough, W.F., Sun, S.-S. (1995). Composition of the Earth. Chem. Geol. 120, 223-53.

Rastsvetaeva et al., (2020). Crystallography Reports, Vol. 65, No. 5, pp. 704–710.

Rudnick, R., Gao, S. (2003). Composition of the continental crust. In Treatise on Geochemistry; Holland, H. D., Turekian, K. K., Eds.; Elsevier-Pergamon: Oxford 3, p. 64.

Severin, K.P. (2004). Energy dispersive spectrometry of rock-forming minerals. Kluwer Academic Publishers.

Schilling, J., Wu, F. Y., McCammon, C., Wenzel, T., Marks, M. A. W., Pfaff, K., Jacob, D. E., & Markl, G. (2011). The compositional variability of eudialyte-group minerals. Mineralogical Magazine, *75*(1), 87-115.